The differentiation and integration of the hippocampal dorsoventral axis are controlled by two nuclear receptor genes

Xiong Yang[1#], Rong Wan[1#], Zhiwen Liu[2,3], Su Feng[2,3], Jiaxin Yang[1], Naihe Jing[2,3*], Ke Tang[1*]

1, Precise Genome Engineering Center, School of Life Sciences, Guangzhou University, Guangzhou, Guangdong 510006, China

2, Guangzhou Laboratory/Bioland Laboratory, Guangzhou, 510005, China

3, CAS Key Laboratory of Regenerative Biology, Guangdong Provincial Key Laboratory of Stem Cell and Regenerative Medicine, Guangdong Institutes of Biomedicine and Health, Chinese Academy of Sciences, Guangzhou 510530, China.

#, Co-first authors

*, Co-corresponding authors

Correspondence: njing@sibcb.ac.cn or ktang.sc@gmail.com.

Abstract

The hippocampus executes crucial functions from declarative memory to adaptive behaviors associated with cognition and emotion. However, the mechanisms of how morphogenesis and functions along the hippocampal dorsoventral axis are differentiated and integrated are still largely unclear. Here, we show that *COUP-TFI* and *-TFII* genes are distinctively expressed in the dorsal and ventral hippocampus, respectively. The loss of *COUP-TFII* results in ectopic CA1/CA3 domains in the ventral hippocampus. The deficiency of *COUP-TFI* leads to the failed specification of dorsal CA1, among which there are place cells. The deletion of both *COUP-TF* genes causes almost agenesis of the hippocampus with abnormalities of trisynaptic circuit and adult neurogenesis. Moreover, *COUP-TFI*/*-TFII* may cooperate to guarantee appropriate morphogenesis and function of the hippocampus by regulating the *Lhx5-Lhx2* axis. Our findings revealed a novel mechanism that *COUP-TFI* and *COUP-TFII* converge to govern the differentiation and integration of distinct characteristics of the hippocampus in mice.

Keywords

Memory; Hippocampus; *COUP-TF* Gene; Place Cell; Trisynaptic Circuit

36 **Introduction**

37 Memory, including declarative and nondeclarative memory, unifies our mental world to
38 ensure the quality of life for people of all ages, from newborns to elderly individuals
39 (Eichenbaum & Cohen, 2014; Kandel, Dudai, & Mayford, 2014). The pioneering studies of
40 Milner and her colleagues revealed that the hippocampus is required for declarative memory
41 but not nondeclarative memory (Penfield & Milner, 1958; Scoville & Milner, 1957). The
42 discovery of activity-dependent long-term potentiation and place cells provides the
43 neurophysiological basis of hippocampal function (Bliss & Lomo, 1973; O'Keefe &
44 Dostrovsky, 1971). The rodent hippocampus can be divided into the dorsal and ventral
45 domains, corresponding to the posterior and anterior hippocampus in humans, respectively.
46 In recent decades, numerous studies have supported the Moser theory that the hippocampus is
47 a heterogeneous structure with distinct characteristics of gene expression, connectivity, and
48 functions along its dorsoventral axis (Bast, 2007; Fanselow & Dong, 2010; Moser & Moser,
49 1998; Strange, Witter, Lein, & Moser, 2014). The dorsal hippocampus, which connects and
50 shares similar gene expression with the neocortex (Fanselow & Dong, 2010), serves the "cold"
51 cognitive function associated with declarative memory and spatial navigation. The ventral
52 hippocampus, which connects and generates similar gene expression with the amygdala and
53 hypothalamus (Cenquizca & Swanson, 2007; Kishi et al., 2000; Pitkanen, Pikkarainen,
54 Nurminen, & Ylinen, 2000), corresponds to the "hot" affective states related to emotion and
55 anxiety (Fanselow & Dong, 2010; Tyng, Amin, Saad, & Malik, 2017). Nonetheless, to date,
56 the molecular and cellular mechanisms by which the morphogenesis, connectivity, and
57 functions along the dorsoventral axis of the hippocampus are differentiated and integrated are
58 largely unknown.

59 The hippocampus, a medial temporal lobe structure in the adult rodent forebrain, originates
60 from the medial pallium (MP) in the medial line of the early dorsal telencephalon. The

cortical hem (CH), which is located ventrally to the MP, functions as an organizer for hippocampal development (Hebert & Fishell, 2008; Schuurmans & Guillemot, 2002). It has been demonstrated that both extrinsic signals, such as *Wnts* and *Bmps*, and intrinsic factors, including *Emx1*, *Emx2*, *Lef1*, *Lhx2*, and *Lhx5*, are involved in the regulation of early morphogenesis of the hippocampus. As the earliest *Wnt* gene to be exclusively expressed in the cortical hem, *Wnt3a* is required for the genesis of the hippocampus (S. M. Lee, Tole, Grove, & McMahon, 2000); in addition, *Lef1* is downstream of Wnt signaling, and the hippocampus is completely absent in $Lef1^{neo/neo}$ null mutant mice (Galceran, Miyashita-Lin, Devaney, Rubenstein, & Grosschedl, 2000). Wnt signaling is essential for early development of the hippocampus. *Emx1* and *Emx2* are mouse homologs of *Drosophila empty spiracles* (Simeone et al., 1992). Interestingly, the dorsal hippocampus is smaller in an *Emx1* null mutant (Yoshida et al., 1997), while *Emx2* is required for the growth of the hippocampus but not for the specification of hippocampal lineages (Tole, Goudreau, Assimacopoulos, & Grove, 2000). Moreover, *Lhx5*, which encodes a LIM homeobox transcription factor and is specifically expressed in the hippocampal primordium, is necessary for the formation of the hippocampus (Zhao et al., 1999). *Lhx2*, encoding another LIM homeobox transcription factor, is required for the development of both the hippocampus and neocortex (Mangale et al., 2008; Monuki, Porter, & Walsh, 2001; Porter et al., 1997). Intriguingly, deficiency of either *Lhx5* or *Lhx2* results in agenesis of the hippocampus, and more particularly, these genes inhibit each other (Hebert & Fishell, 2008; Mangale et al., 2008; Roy, Gonzalez-Gomez, Pierani, Meyer, & Tole, 2014; Zhao et al., 1999), indicating that the *Lhx5* and *Lhx2* genes may generate an essential regulatory axis to ensure the appropriate hippocampal development. Nevertheless, whether there are other intrinsic genes that participate in the regulation of morphogenesis and function of the hippocampus has not been fully elucidated.

COUP-TF genes, including *COUP-TFI* (also known as *NR2F1*) and *COUP-TFII* (also known as *NR2F2*), encode two transcription factor proteins belonging to the nuclear receptor superfamily (Yang, Feng, & Tang, 2017). Mutations of *COUP-TFI* are highly related to neurodevelopmental disorders (NDD), such as intellectual disability (ID) and autism spectrum disorders (ASD) (Bertacchi et al., 2020; Bosch et al., 2014; Contesse, Ayrault, Mantegazza, Studer, & Deschaux, 2019), and mutations of the *COUP-TFII* gene are associated with congenital heart defects (CHD) (Al Turki et al., 2014). By using animal models, our studies and others have demonstrated that *COUP-TF* genes participate in the regulation of the development of the central nervous system (Zhang et al., 2020). The *COUP-TFI* plays an essential role in the differentiation of cortical excitatory projection neurons and inhibitory interneurons, the development of the dorsal hippocampus, and cortical arealization (Armentano et al., 2007; Bertacchi et al., 2020; Del Pino et al., 2020; J. Feng et al., 2021; Flore et al., 2017; Lodato et al., 2011; C. Zhou et al., 1999; C. Zhou, Tsai, & Tsai, 2001). *COUP-TFII* plays a vital role in the development of the amygdala, hypothalamus, and cerebellum (S. Feng et al., 2017; Kim, Takamoto, Yan, Tsai, & Tsai, 2009; Tang, Rubenstein, Tsai, & Tsai, 2012). Nevertheless, whether and how *COUP-TFI* and/or *COUP-TFII* genes regulate the differentiation and integration of hippocampal morphogenesis, connectivity, and function is still largely unclear.

Here, our data show that *COUP-TFI* and *-TFII* genes are differentially expressed along the dorsoventral axis of the postnatal hippocampus. The loss of *COUP-TFII* results in ectopic CA1 and CA3 domains in the ventral hippocampus. In addition, the deficiency of *COUP-TFI* leads to not only dysplasia of the dorsal hippocampus but also failed specification and differentiation of the dorsal CA1 pyramidal neuron lineage. Furthermore, the deletion of both genes in the $RX^{Cre/+}$; $COUP\text{-}TFI^{F/F}$; $COUP\text{-}TFII^{F/F}$ double mutant mouse causes almost agenesis of the hippocampus, accompanied by compromised specification of the CA1, CA3,

and dentate gyrus (DG) domains. The components of the trisynaptic circuit are abnormal in the corresponding single-gene or double-gene mutant model. Moreover, *COUP-TF* genes may cooperate to guarantee the appropriate morphogenesis and function of the hippocampus by regulating the *Lhx5-Lhx2* axis.

Results

Differential expression profiles of *COUP-TFI* and -*TFII* genes along the dorsoventral axis in the developing and postnatal hippocampus

To investigate the functions of the *COUP-TFI* and *COUP-TFII* genes in the hippocampus, immunofluorescence staining was first performed to examine their expression in wild-type mice at postnatal month 1 (1M). In both the coronal and sagittal sections, COUP-TFI exhibited a septal/dorsal high-temporal/ventral low expression pattern along the hippocampus (Figure 1Aa, d, c, f, g, j, m, i, l, and o), and its expression is highest in the dorsal CA1 region (Figure 1Aa, d, c, f, j, and l), where place cells are mainly located (O'Keefe & Conway, 1978; O'Keefe & Dostrovsky, 1971), and the dorsal DG, where there are adult neural stem cells (NSCs) (Gould & Cameron, 1996). However, the expression of COUP-TFII was high in the temporal/ventral hippocampus but was barely detected in the septal/dorsal part of the hippocampus (Figure 1Ab, c, e, f, h, i, k, l, n, and o). The dorsal-high COUP-TFI and ventral-high COUP-TFII expression profiles were further verified in the postnatal hippocampi at 1M by western blotting assays (Figure 1Ap, q). At embryonic day 10.5 (E10.5), COUP-TFI was detected in the dorsal pallium (DP) laterally and COUP-TFII was expressed in the MP and CH medially (Figure 1—figure supplement 1Aa-b). At E11.5 and E12.5, the expression of COUP-TFII remained in the CH (Figure 1—figure supplement 1Ac-d, Bb-c). Interestingly, COUP-TFI and -TFII generated complementary expression patterns in the hippocampal primordium with COUP-TFI in the dorsal MP and COUP-TFII in the ventral CH at E14.5

135 (Figure 1—figure supplement 1Ba-f). Additionally, septal/dorsal-high COUP-TFI and
136 temporal/ventral-high COUP-TFII expression patterns were observed at postnatal day 0 (P0)
137 (Figure 1—figure supplement 1Bg-l). The data above revealed that the differential expression
138 patterns of *COUP-TFI* and *-TFII* genes were generated and maintained along the
139 dorsoventral axis in the early hippocampal primordium, the developing and postnatal
140 hippocampus, indicating that they could play distinct roles in the mediation of the
141 morphogenesis and functions of the hippocampus.

142 Next, to investigate the roles of *COUP-TF* genes in the hippocampus, an *RXCre* mouse was
143 used to excise the expression of the *COUP-TFI* and/or *COUP-TFII* genes (Swindell et al.,
144 2006; Tang et al., 2012). The deletion efficiency of RXCre recombinase was verified by
145 immunofluorescence assays. Compared with control mice, either *COUP-TFII* or *COUP-TFI*
146 could be excised in the postnatal hippocampus of corresponding single-gene mutants at 1M
147 (Figure 1—figure supplement 1Ca-i). In addition, compared with control mice, both the
148 *COUP-TFI* and *-TFII* genes were almost completely deleted in the hippocampal primordium
149 in mutant mice at E14.5 (Figure 1—figure supplement 1Cj-o). Since the LacZ expression
150 serves as an indicator for the deletion of *COUP-TFII* (Swindell et al., 2006; Tang et al.,
151 2012), we performed immunofluorescence staining with antibodies against COUP-TFII and
152 LacZ on the sagittal sections of $RX^{Cre/+}$; $COUP\text{-}TFII^{F/+}$ and $RX^{Cre/+}$; $COUP\text{-}TFII^{F/F}$ mice at
153 E11.5. COUP-TFII was readily detected at the hippocampal primordium of the heterozygous
154 mutant embryo at E11.5 (Figure 1—figure supplement 1Da, c, g); in contrast, the expression
155 of *COUP-TFII* was significantly reduced in the homozygous mutant (Figure 1—figure
156 supplement 1Dd, f, j). In addition, compared with the heterozygous mutant embryo (Figure
157 1—figure supplement 1Db-c, h), the LacZ signals clearly increased in the hippocampal
158 primordium of the homozygous mutant embryo at E11.5 (Figure 1—figure supplement 1De-f,
159 k), suggesting that RX-Cre recombinase can efficiently excise the *COUP-TFII* gene in the

160 hippocampal primordium as early as E11.5. Intriguingly, we observed that the expression of
161 *COUP-TFI* increased in the caudal hippocampal primordium of the *COUP-TFII* homozygous
162 mutant embryo at E11.5 (Figure 1—figure supplement 1Di, l), indicating that similar to the
163 observations in the early optic cup (Tang et al., 2010), *COUP-TFI* and *-TFII* genes could be
164 partially compensate with each other in the developing hippocampal primordium. All the data
165 above show that RXCre recombinase could efficiently excise *COUP-TFI* and/or *COUP-TFII*
166 in the early developing and postnatal hippocampus.
167

168 **The *COUP-TFII* gene is required for the appropriate morphogenesis of the ventral**
169 **hippocampus but not of the dorsal hippocampus**

170 Given that the *COUP-TFII* gene is highly and specifically expressed in the postnatal ventral
171 hippocampus and the CH of the hippocampal primordium (Figure 1 and Figure 1—figure
172 supplement 1), we asked whether the *COUP-TFII* gene is required for the appropriate
173 morphogenesis of the hippocampus, particularly the ventral hippocampus. To answer this
174 question, we conducted Nissl staining with samples from the *COUP-TFII* single-gene
175 ($RX^{Cre/+}$; $COUP\text{-}TFII^{F/F}$ or $RX^{Cre/+}$; $CII^{F/F}$) knockout mouse model. In coronal sections,
176 compared with the control at 1M, the septal hippocampus was normal; unexpectedly, an
177 ectopic CA-like region was observed medially in the temporal hippocampus in the *COUP-*
178 *TFII* mutant, where the prospective posterior part of the medial amygdaloid (MeP) nucleus
179 was situated, indicated by the star (Figure 1Ba-f). The presence of the ectopic CA-like region
180 in the ventral but not dorsal hippocampus of the mutant was further confirmed by the
181 presence of the prospective MeP and amygdalohippocampal area (AHi) in sagittal sections,
182 as indicated by the star (Figure 1Bg-l). Furthermore, immunofluorescence assays were
183 performed to verify whether specific lineages of the hippocampus were altered with sagittal
184 sections, in which the subregions of both the dorsal and ventral hippocampus were well

185 displayed and distinguished. Ctip2 is a marker for CA1 pyramidal neurons and DG granule
186 neurons, and HuB is a marker for CA3 pyramidal cells (Sugiyama, Osumi, & Katsuyama,
187 2014). The dorsal hippocampus appeared normal in both the control and mutant mice at 1M
188 (Figure 1Ca-l). Nonetheless, compared with the observations in control mice, an ectopic
189 HuB-positive CA3 pyramidal neuron lineage, indicated by the star, and a duplicated Ctip2-
190 positive CA1 pyramidal neuron lineage, indicated by the arrowhead, were observed in the
191 ventral hippocampal area in the mutant (Figure 1Ca-f, m-r), revealing that there were ectopic
192 CA1 and CA3 lineages in the *COUP-TFII* mutants.
193 Consistent with the previous report (Leid et al., 2004), the expression of Ctip2 was detected
194 in the amygdala including the AHi and posteromedial cortical amygdaloid nucleus (PMCo);
195 in addition, Ctip2 was also highly expressed in the dorsal part of the MeP (MePD) in the
196 control (Figure 1Cb, n).
197 Intriguingly, compared with the controls at 1M, there were ectopic CA domains in the mutant
198 ventral hippocampus with the expense of the Ctip2 positive AHi and MePD amygdaloid
199 nuclei (Figure 1Ce, q), indicated by the arrows. Clearly, all the data above suggested that the
200 *COUP-TFII* gene is necessary to ensure the appropriate morphogenesis of the ventral
201 hippocampus.
202 At early embryonic stages, *COUP-TFII* was preferentially expressed in the CH (Figure 1—
203 figure supplement 1Ab, d, 1Bb, e), the organizer of the hippocampus, and at postnatal 1-
204 month-old (1M) stage, *COUP-TFII* was also highly expressed in some amygdala nuclei such
205 as the AHi and medial amygdaloid nucleus, which are adjacent to the ventral/temporal
206 hippocampus (Figure 1Ae, h, n) (Tang et al., 2012). We would like to investigate the
207 correlation of the CH and/or amygdala anlage with the duplicated ventral hippocampal
208 domains in the *COUP-TFII* mutant in detail in our future study. The observations above
209 suggest that *COUP-TFII* is not only specifically expressed in the ventral hippocampus but is

210 also required for morphogenesis and probably the function of the ventral hippocampus. Since
211 the ventral hippocampus participates in the regulation of emotion and stress, mutations in the
212 *COUP-TFII* gene lead to CHDs, and the formation of the ventral hippocampus is disrupted in
213 *COUP-TFII* mutant mice at 1M, we wondered whether CHD patients with *COUP-TFII*
214 mutations also exhibit symptoms associated with psychiatric disorders such as depression,
215 anxiety, or schizophrenia.
216
217 **The *COUP-TFI* gene is required for the specification and differentiation of the dorsal**
218 **CA1 identity**
219 Next, we asked whether the deletion of the *COUP-TFI* gene by *RX-Cre* also affected the
220 development of the hippocampus. Consistent with the previous finding in $Emx1^{Cre/+}$; *COUP-*
221 $TFI^{F/F}$ mutant mice (Flore et al., 2017), it was the septal/dorsal hippocampus, not the
222 temporal/ventral hippocampus, that was specifically shrunken in both coronal (Figure 2Aa-f)
223 and sagittal sections (Figure 2Ag-i) of $RX^{Cre/+}$; $COUP\text{-}TFI^{F/F}$ ($RX^{Cre/+}$; $CI^{F/F}$) mutant mice.
224 Then, we asked whether the loss of the *COUP-TFI* gene caused abnormal specification and
225 differentiation of hippocampal lineages. Compared with the control mice, *COUP-TFI* mutant
226 mice had fewer HuB-positive CA3 pyramidal neurons, as indicated by the star; intriguingly,
227 Ctip2-positive CA1 pyramidal neurons failed to be detected, as indicated by the arrowhead,
228 with Ctip2-positive DG granule neurons unaltered in the dorsal hippocampus (Figure 2Ba-l).
229 The loss of the dorsal CA1 pyramidal neuron identity in mutant mice was further confirmed
230 by Wfs1, another dorsal CA1 pyramidal neuron-specific marker (Takeda et al., 2001) (Figure
231 2Ca-r). Nonetheless, the HuB-positive and Ctip2-positive lineages were comparable in the
232 ventral hippocampus between the control and mutant mice (Figure 2Ba-f, m-r), even though
233 the low expression of COUP-TFI was detected there. Indeed, *COUP-TFI* is not only
234 expressed at the highest level in the dorsal CA1 but is also required for the specification and

differentiation of dorsal CA1 pyramidal neurons, among which place cells are essential for learning and memory (O'Keefe & Conway, 1978; O'Keefe & Dostrovsky, 1971).

Given that dysplasia of the dorsal hippocampus was generated in both the *Emx1-Cre* and *RX-Cre* models (Flore et al., 2017) (Figure 2Aa-l), we asked whether the development of dorsal CA1 pyramidal neurons was also abolished in *Emx1*$^{Cre/+;}$ *COUP-TFI*$^{F/F}$ mutant mice. To answer this question, immunofluorescence staining was conducted first. Compared with that in the control mice, the proportions of either the Wfs1- or Ctip2-positive CA1 domain were reduced in the mutant mice at 3M (Figure 2—figure supplement 1Aa-h), indicating that the differentiation of the dorsal CA1 pyramidal neurons was also compromised in the *Emx1-Cre* model, although it was less severe than that in the *RX-Cre* model. To make our findings more consistent with previous studies, we further conducted experiments with the *Emx1-Cre* model. Afterward, to investigate the fine structure of the dorsal CA1 pyramidal neurons, Golgi staining was performed. Compared with those of control mice, the numbers of secondary dendrites and branch points of both the apical and basal dendrites were significantly reduced in the dorsal CA1 pyramidal neurons of mutant mice at 3M (Figure 2—figure supplement 1Ba-e). Then, the dorsal hippocampus-related spatial learning and memory behavior test, the Morris water maze, was performed (Vorhees & Williams, 2006). Consistent with a previous report (Flore et al., 2017), spatial learning and memory function was significantly impaired in adult *Emx1*$^{Cre/+}$; *COUP-TFI*$^{F/F}$ mice, compared with the control mice (Figure 2—figure supplement 1C). The data above suggest that *COUP-TFI* is vital for the morphogenesis, lineage specification, and spatial learning and memory of the dorsal hippocampus, and particularly, the compromised dorsal CA1 lineage could contribute to the phenotypes associated with neurodevelopmental disorders, including ID or ASD.

The *COUP-TFI* and -*TFII* genes coordinate to ensure the genesis of the hippocampus

260 Given that the loss of either *COUP-TFI* or *-TFII* leads to dysplasia of the dorsal or ventral
261 hippocampus, respectively, we asked whether these genes compensate for each other to
262 regulate the morphogenesis of the hippocampus. To answer this question, the $RX^{Cre/+}$; *COUP-*
263 $TFI^{F/F}$; $COUP\text{-}TFII^{F/F}$ ($RX^{Cre/+}$; $CI^{F/F}$; $CII^{F/F}$) double-mutant mouse was generated, and a few
264 homozygous double-gene mutant mice survived for approximately 3 weeks (3W).
265 Nonetheless, the reason for the lethality of the double-mutant mice is still unknown. Nissl
266 staining data showed that compared with that of control mice, the septal hippocampus was
267 severely shrunken, as indicated by the star, and the temporal hippocampus was barely
268 observed in the double-mutant mouse brains (Figure 3Aa-h). Unexpectedly, an ectopic
269 nucleus was observed in the region of the prospective temporal hippocampus, indicated by
270 the arrowhead, in the double-mutant mice (Figure 3Ag-h). In addition, compared with those
271 of controls, the regions with HuB-positive CA3 pyramidal neurons and Ctip2-positive or
272 Prox1-positive DG granule neurons were diminished in the double mutants; in particular,
273 Ctip2-positive dorsal CA1 pyramidal neurons could not be detected in the double mutants
274 (Figure 3Ba-l). Furthermore, compared with the domains of controls, no HuB-positive, Ctip2-
275 positive, or Prox1-positive domains could be detected in the prospective temporal
276 hippocampus in the double mutants (Figure 3Ca-l). The results above suggest that the *COUP-*
277 *TFI* and *COUP-TFII* genes coordinate with each other to mediate the appropriate
278 morphogenesis of the entire hippocampus.
279

280 ***COUP-TF* genes and adult neurogenesis in the hippocampus**

281 Given that the *COUP-TFI* or *-TFII* gene was highly expressed in the dorsal or ventral DG,
282 respectively (Figure 1A), and that RX-Cre recombinase could efficiently delete either gene in
283 the DG (Figure 1—figure supplement 1Ca-i), we asked whether the loss of the *COUP-TFI*
284 or/and *-TFII* gene in the DG would affect hippocampal adult neurogenesis. To answer this

285 question, the ventral DG, dorsal DG, and septal DG were chosen to perform
286 immunofluorescence assays in the *COUP-TFII* mutant, *COUP-TFI* mutant, and double
287 mutant models, respectively. Adult NSCs in the subgranular zone (SGZ) of the DG express
288 both GFAP and Nestin, and newborn granule neurons express Dcx (Gao, Arlotta, Macklis, &
289 Chen, 2007). The numbers of NSCs and newborn neurons in the SGZ of the DG were
290 comparable between control mice and either the *COUP-TFII* or *COUP-TFI* mutant mice
291 (Figure 3—figure supplement 1Aa-p, Ba-h); nonetheless, compared with those of control
292 mice, the numbers of the NSCs and newborn granule neurons in the SGZ of the DG were
293 reduced in the double mutants (Figure 3—figure supplement 1Aq-x, Bi-l), and the reduction
294 in both lineages was significant (Figure 3—figure supplement 1Ca, b). The data above
295 suggest that *COUP-TF* genes may coordinate with each other to execute essential functions
296 for appropriate hippocampal adult neurogenesis in the DG.
297
298 **Hippocampal trisynaptic connectivity was impaired in postnatal *COUP-TFII* single-,**
299 ***COUP-TFI* single-, and double-mutant mice at about 1M**
300 Given that dysplasia of the hippocampus was observed in all three mouse models, we asked
301 whether the connectivity of the hippocampal trisynaptic circuit associated with the DG, CA3,
302 and CA1 regions (Amaral, 1993) was normal in these models. To answer this question, the
303 components of the trisynaptic circuit were characterized in the ventral hippocampus of
304 *COUP-TFII* mutants, the dorsal hippocampus of *COUP-TFI* mutants, and the septal
305 hippocampus of double mutants. Calretinin is a marker of mossy cells, Calbindin is a marker
306 of mossy fibers, and SMI312 is a marker of Schafer collaterals (Flore et al., 2017). Compared
307 with those of controls (Figure 4Aa, b, e, f, i, and j), the numbers of Calretinin-positive mossy
308 cells were reduced, Calbindin-positive mossy fibers were longer but thinner, and SMI312-
309 positive Schafer collaterals were thinner and discontinued in the ventral hippocampus of

310 *COUP-TFII* mutants at 1M (Figure 4Ac, d, g, h, k, and l). In addition, similar to the previous
311 report (Flore et al., 2017), the numbers of Calretinin-positive mossy cells were decreased,
312 Calbindin-positive mossy fibers were shorter and thinner, and SMI312-positive Schafer
313 collaterals were barely detected in the dorsal hippocampus of *COUP-TFI* mutants (Figure
314 4Ac, d, g, h, k, and l), compared with those of controls at 1M (Figure 4Ba, b, e, f, i, and j).
315 Moreover, compared with those of control mice (Figure 4Ca, b, e, f, i, and j), the numbers of
316 Calretinin-positive mossy cells were reduced; both Calbindin-positive mossy fibers and
317 SMI312-positive Schafer collaterals were barely detected in the prospective septal
318 hippocampus of the double mutants at 3W (Figure 4Cc, d, g, h, k, and l). Clearly, without
319 both *COUP-TF* genes, the connectivity of the hippocampal trisynaptic circuit was abolished
320 more severely. The observations above revealed that the formation of the trisynaptic circuit,
321 which is one of the fundamental characteristics of hippocampal neurophysiology (Basu &
322 Siegelbaum, 2015), was abnormal in all three mouse models, indicating that both the
323 morphology and functions of the hippocampus are most likely compromised in the loss of the
324 *COUP-TFI* and/or *COUP-TFII* gene.
325
326 **The expression of several essential regulatory genes associated with early hippocampal**
327 **development was abnormal in double mutants**
328 Given that the hippocampus was almost completely diminished in double mutants, we asked
329 how *COUP-TF* genes participated in the regulation of the early morphogenesis of the
330 hippocampus. To answer this question, total RNA isolated from the whole telencephalons of
331 control (n=5) and double-mutant-(n=3) embryos at E11.5 was used to generate cDNA, and
332 then real-time quantitative PCR (RT-qPCR) assays were performed. As expected, compared
333 with that of control mice, the expression of *COUP-TFI* and *COUP-TFII* was reduced
334 significantly in the double mutant mice (Figure 5A). Then, we mainly focused on the intrinsic

regulatory networks by analyzing the expression profiles of two groups of transcription factor genes. The *Foxg1*, *Gli3*, *Lhx2*, *Otx1, Otx2*, and *Pax6* genes, which are highly related to the early patterning of the dorsal telencephalon (Hebert & Fishell, 2008), were in the first group; *Axin2*, *Emx1*, *Emx2*, *Lef1*, *Lhx5*, and *Tcf4* genes, which are associated with early hippocampal development (Galceran et al., 2000; Moore & Iulianella, 2021; Tole et al., 2000; Yoshida et al., 1997; Zhao et al., 1999), were in the other group. The expression of the *Foxg1*, *Gli3*, *Lhx2*, *Otx1, Otx2*, and *Pax6* genes was comparable between the controls and double mutants (Figure 5A), indicating that the early patterning of the dorsal telencephalon is largely unaltered. Compared with that of control mice, the expression of the *Axin2*, *Emx2*, *Lef1*, and *Tcf4* genes was normal in the double mutants; interestingly, the expression of the *Emx1* and *Lhx5* transcripts was decreased significantly in the double mutants at E11.5 compared to that in control mice (Figure 5A). Consistent with the downregulated expression of *Lhx5* transcripts in the double mutant, the expression of the Lhx5 protein was reduced in the CH in the double mutants at E11.5; moreover, the number of Lhx5-positive Cajal-Retzius cells decreased in the double mutant embryos at E11.5, E13.5 and E14.5 (Figure 5Ba-d, a'-d', a''-d'', i-l, i'-l', q-t, q'-t'). The expression of *Lhx2* was expanded ventrally into the choroid plexus in the *Lhx5* null mutant mice (Zhao et al., 1999), indicating that *Lhx5* could inhibit *Lhx2* expression locally. Consistent with RT-qPCR data, the expression of Lhx2 was comparable between the control and double-mutant mice at E11.5 (Figure 5Be-h, e'-h'). Interestingly, the expression of the Lhx2 protein was increased in the hippocampal primordium in the *COUP-TF* double-mutant mice at E13.5 and E14.5 (Figure 5Bm-p, m'-p', u-x, u'-x'). The upregulation of Lhx2 expression is most likely associated with the reduced expression of the *Lhx5* gene.

Next, we asked whether neural precursor cells (NPCs), intermediate progenitor cells (IPCs), or newborn neurons were affected in the early development of the hippocampus in double-

mutant mice. Sox2 is a marker for NPCs, Tbr2 is a marker for IPCs, and NeuroD1 is a marker for newborn neurons (Yu, Marchetto, & Gage, 2014). The expression of Sox2 in the hippocampal regions was comparable between the control and double-mutant mice at E14.5 (Figure 5Ca-d, a'-d'), indicating that the generation of NPCs was normal. Nevertheless, compared with the control embryos, the numbers of Tbr2-positive IPCs and NeuroD1-positive newborn neurons were reduced in the double-mutant embryos (Figure 5Ce-l, e'-l'), and the reduction was significant (Figure 5D). Our observations were consistent with previous findings in *Lhx5* null mutant mice that the specification of the hippocampal NPCs was normal, but the later differentiation event was abolished (Zhao et al., 1999). All the data above suggest that *COUP-TF* genes may cooperate to ensure the early morphogenesis of the hippocampus by regulating the appropriate expression levels of *Lhx5* and *Lhx2* genes. Nevertheless, we could not exclude other possibilities that *COUP-TF* genes could also participate in the modulation of hippocampal development through *Emx1* or other genes.

Discussion

In our present study, we observed dorsal-high COUP-TFI and ventral-high COUP-TFII expression profiles in the postnatal hippocampus. The deletion of the *COUP-TFII* gene led to duplicated CA1 and CA3 domains of the ventral hippocampus. The loss of *COUP-TFI* resulted in the failed specification and differentiation of the dorsal CA1 pyramidal neuron lineage with a diminished dorsal hippocampus. Furthermore, the deficiency of both *COUP-TF* genes caused atrophy of almost the entire hippocampus, accompanied by compromised generation of the CA1, CA3, and DG identities. In addition, the dorsal trisynaptic components, ventral trisynaptic components, or entire trisynaptic components were abolished in the corresponding *COUP-TFI* gene mutant, *COUP-TFII* gene mutant, or *COUP-TFI*/*-TFII* double-gene mutant mice. Moreover, *COUP-TF* genes may cooperate to ensure the

385 appropriate morphogenesis and function of the hippocampus by regulating the *Lhx5-Lhx2*
386 axis.
387
388 **1. *COUP-TFII* governs the distinct characteristics of the ventral hippocampus**
389 Sixty years ago, the pioneering work of Milner and her colleagues discovered the essential
390 role of the hippocampus in declarative memory (Penfield & Milner, 1958; Scoville & Milner,
391 1957). Recently, accumulating evidence has supported the Moser theory that the
392 hippocampus is a heterogeneous structure with distinct characteristics of gene expression,
393 connectivity, and function along its dorsoventral axis (Bast, 2007; Fanselow & Dong, 2010;
394 Moser & Moser, 1998; Strange et al., 2014). The dorsal hippocampus marked in blue, in
395 which gene expression is similar to the neocortex, serves the "cold" cognitive function
396 associated with declarative memory and spatial navigation, and the ventral hippocampus
397 marked in red, in which gene expression is close to the hypothalamus and amygdala,
398 corresponds to the "hot" affective states related to emotion and anxiety (Figure 5—figure
399 supplement 1). The ventral hippocampus generates direct connectivity with the amygdala,
400 hypothalamus, medial prefrontal cortex (mPFC), and olfactory bulb (Cenquizca & Swanson,
401 2007; Hoover & Vertes, 2007; Kishi et al., 2000; Pitkanen et al., 2000; Roberts et al., 2007).
402 Nonetheless, thus far, the molecular and cellular mechanism of how the morphogenesis,
403 connectivity, and function of the ventral hippocampus is achieved has been largely unclear.
404 *COUP-TFII*, a nuclear receptor gene associated with heart disease(Al Turki et al., 2014)
405 (High et al., 2016), was highly and exclusively expressed in the ventral hippocampus in 1-
406 month-old mice and was expressed ventrally in the CH of the hippocampal primordium in
407 mouse embryos (Figure 1, Figure 1—figure supplement 1, Figure 5Ea), indicating that the
408 *COUP-TFII* gene may participate in the regulation of the development and function of the
409 ventral hippocampus. First, deficiency of the *COUP-TFII* gene led to the duplication of the

410 CA1 and CA3 domains of the ventral hippocampus but not the dorsal hippocampus, which
411 was confirmed both morphologically and molecularly (Figure 1). Second, the formation of
412 the trisynaptic circuit was specifically abolished in the ventral hippocampus of *COUP-TFII*
413 mutants (Figure 4), indicating that the intrahippocampal circuit, information transfer, and
414 function of the ventral hippocampus could be compromised. Third, the ventral hippocampus
415 generates neural circuits with the mPFC, amygdala, nucleus accumbens, and hypothalamus,
416 which are associated with anxiety/behavioral inhibition, fear processing, pleasure/reward
417 seeking, and the neuroendocrine system, respectively (Anacker & Hen, 2017; Baik, 2020;
418 Bryant & Barker, 2020; Cenquizca & Swanson, 2007; Herman et al., 2016; Kishi et al., 2000;
419 O'Leary & Cryan, 2014; Pitkanen et al., 2000). These ventral hippocampal projections may
420 be important for processing information related to emotion and anxiety. Intriguingly, our
421 previous studies revealed that *COUP-TFII* is required for the development of the
422 hypothalamus, amygdala, and olfactory bulb (S. Feng et al., 2017; Tang et al., 2012; X. Zhou
423 et al., 2015), all of which generate functional neural circuits with the ventral hippocampus
424 (Fanselow & Dong, 2010). Particularly, both the hypothalamus and amygdala are also
425 diminished in $RX^{Cre/+}$; $COUP\text{-}TFII^{F/F}$ mutant mice (S. Feng et al., 2017; Tang et al., 2012),
426 indicating that their interconnectivities with the ventral hippocampus are abnormal. Thus, all
427 the findings above suggest that *COUP-TFII* is a novel and essential intrinsic regulator that
428 controls the morphogenesis, connectivity, and function of the ventral hippocampus.

429 Given that mutations of *COUP-TFII* are highly associated with CHDs (Al Turki et al.,
430 2014), the expression of *COUP-TFII* is also confined to the ventral hippocampus in human
431 embryos (Alzu'bi et al., 2017), and *COUP-TFII* gene is required for the distinct
432 characteristics of the ventral hippocampus in mouse (Figure 1, Figure 4), we wondered
433 whether CHD patients carrying mutations of *COUP-TFII* also display symptoms of
434 psychiatric disorders, such as depression, anxiety, or schizophrenia, related to the ventral

435 hippocampus. In our future study, we would like to generate hippocampus-specific or
436 hippocampal subdomain-specific conditional knockout models to dissect distinct roles of the
437 *COUP-TFII* gene in the hippocampus, particularly in the ventral hippocampus, in detail.
438

439 **2. The *COUP-TFI* gene is required for the specification and differentiation of dorsal**
440 **CA1 pyramidal neurons**

441 The expression of *COUP-TFI*, another orphan nuclear receptor gene associated with
442 neurodevelopmental disorders (Bertacchi et al., 2020; Bosch et al., 2014; Contesse et al.,
443 2019), is high in the dorsal MP of the hippocampal primordium and is higher in the dorsal
444 hippocampus than in the ventral hippocampus (Figure 1, Figure 1—figure supplement 1,
445 Figure 5Ea) (Flore et al., 2017). Consistent with previous observations in $Emx1^{Cre/+}$; *COUP-*
446 $TFI^{F/F}$ mutant mice (Flore et al., 2017), the dorsal hippocampus but not the ventral
447 hippocampus was specifically shrunken in $RX^{Cre/+}$; $COUP\text{-}TFI^{F/F}$ mice (Figure 2, Figure 5—
448 figure supplement 1). *COUP-TFI* is expressed at the highest level in dorsal CA1 pyramidal
449 neurons (Figure 1), indicating that the *COUP-TFI* gene may play a role in the specification
450 and differentiation of dorsal CA1 pyramidal neurons. As expected, the expression of Ctip2
451 and Wfs1, two markers for dorsal CA1 pyramidal neurons, could not be detected in the
452 prospective dorsal CA1 domain in $RX^{Cre/+}$; $COUP\text{-}TFI^{F/F}$ mutant mice (Figure 2);
453 furthermore, $Emx1^{Cre/+}$; $COUP\text{-}TFI^{F/F}$ mutant mice partially phenocopied the compromised
454 development of the dorsal CA1 lineage (Figure 2—figure supplement 1). It seems that the
455 spatiotemporal activity of RX-Cre recombinase is better or broader than that of the Emx1-Cre
456 recombinase during the critical period of the specification of the dorsal CA1 pyramidal
457 neuron identity. In addition, the Golgi staining assay revealed that the development of the
458 dendrites of the dorsal CA1 pyramidal neurons was abnormal (Figure 2—figure supplement
459 1). All the observations above indicate that the *COUP-TFI* gene is not only necessary for the

460 morphogenesis of the dorsal hippocampus but is also required for the specification and
461 differentiation of the dorsal CA1 pyramidal neurons, among which there are place cells. The
462 identification of place cells fifty years ago was one of the most important breakthroughs in
463 understanding the role of the hippocampus in memory (O'Keefe & Dostrovsky, 1971). Except
464 for spatial information, place cells in the dorsal CA1 may also encode nonspatial
465 representations, such as time (Eichenbaum, 2017; Lisman et al., 2017). Notably, 95% of
466 patients carrying *COUP-TFI* mutations are associated with ID. Here, our observations
467 support the notion that the *COUP-TFI* gene is a novel intrinsic regulator that specifies the
468 dorsal CA1 pyramidal cell identity, which will benefit the understanding of both
469 neurophysiological functions of the hippocampus and the etiology of NDD including ID and
470 ASD.
471

472 **3. *COUP-TFI* and *-TFII* cooperate to ensure the appropriate morphogenesis of the**
473 **hippocampus by regulating the *Lhx5-Lhx2* axis in mice**

474 In wild-type mice, *COUP-TFI* and *-TFII* genes generated complementary expression profiles
475 in the embryonic hippocampal primordium with *COUP-TFI* in the dorsal MP, marked in
476 green; *COUP-TFII* in the ventral CH, marked in red (Figure 5Ea, Figure 1—figure
477 supplement 1); and in the postnatal hippocampus with high-COUP-TFI expression in the
478 dorsal, marked in green; and high-COUP-TFII expression in the ventral, marked in red
479 (Figure 5Ea, Figure 1). These findings indicated that *COUP-TF* genes may coordinate to
480 regulate hippocampal development. Indeed, as discussed above, the loss of either *COUP-TFI*
481 or *-TFII* only leads to dysplasia of the dorsal hippocampus (Flore et al., 2017) (Figure 2,
482 Figure 2—figure supplement 1) or ventral hippocampus (Figure 1), respectively; intriguingly,
483 while both genes are efficiently excised by *RX-Cre* in the hippocampal primordium (Figure
484 1—figure supplement 1), more severely shrunken hippocampi developed in the 3-week-old

485 double knockout mice (Figure 3). The dosage-dependent severity of hippocampal
486 abnormalities suggested that two nuclear receptor genes, *COUP-TFI* and *-TFII* could
487 cooperate with each other to execute an essential and intrinsic function in the development of
488 the hippocampus.

489 It is known that both extrinsic signals and intrinsic factors participate in the regulation of the
490 early development of the hippocampus. Notably, mutations of *Wnt3a* and *Lef1* eliminate the
491 entire hippocampus (Galceran et al., 2000; S. M. Lee et al., 2000). Given that the expression
492 of *Axin2*, *Lef1* and *Tcf4*, three Wnt-responsive transcription factor genes, was not altered in
493 the *COUP-TF* double mutant (Figure 5A), it is unlikely that abnormal Wnt signaling is the
494 cause of the compromised hippocampus. *Lhx5* is specifically expressed in the hippocampal
495 primordium and is required for the morphogenesis of the hippocampus (Zhao et al., 1999).
496 *Lhx2* is necessary for hippocampal development by repressing cortical hem fate (Mangale et
497 al., 2008; Monuki et al., 2001). Agenesis of the hippocampus is observed in either *Lhx5* or
498 *Lhx2* null mutant mice, and these genes particularly repress each other (Hebert & Fishell,
499 2008; Mangale et al., 2008; Roy et al., 2014; Zhao et al., 1999), indicating that the proper
500 expression levels of *Lhx5* and *Lhx2* genes are critical to maintain the appropriate
501 development of the hippocampus (Figure 5Eb). The transcriptional and protein expression
502 levels of *Lhx5* but not *Lhx2* were first reduced in the hippocampal primordium of *COUP-TF*
503 double-mutant mice at E11.5; later, enhanced expression of the Lhx2 protein was detected in
504 the hippocampal primordium of double-mutant mice at E13.5 and E14.5 (Figure 5A-B).
505 Moreover, the number of Lhx5-positive Cajal-Retzius cells was clearly reduced in the double
506 mutant embryos at E11.5, E13.5 and E14.5; consistent with the observations in the *Lhx5* null
507 mutant (Li et al., 2021; Miquelajáuregui et al., 2010), the generation of Sox2-positive
508 hippocampal NPCs was not affected, but the development of Tbr2-positive IPCs and
509 NeuroD1-positive newborn neurons was abnormal in *COUP-TF* double-mutant mice (Figure

510 5). Thus, our findings reveal a novel intrinsic regulatory mechanism that *COUP-TFI* and
511 *COUP-TFII*, two disease-associated nuclear receptor genes, may cooperate with each other to
512 ensure proper hippocampal morphogenesis by regulating the *Lhx5-Lhx2* axis. Intriguingly,
513 compared with the adult *Emx1*$^{Cre/+}$; *COUP-TFI*$^{F/F}$ mutant mice, the hippocampus was much
514 smaller in the adult *Emx1*$^{Cre/+}$; *COUP-TFI*$^{F/F}$; *COUP-TFII*$^{F/F}$ double-gene mutant mice;
515 nevertheless, both the dorsal and ventral hippocampus were readily detected in double-gene
516 mutants with *Emx1-Cre* (our unpublished observations). In addition, the discrepancy between
517 the shrunken dorsal hippocampus associated with the loss of *COUP-TFI* and the duplicated
518 CA domains of the ventral hippocampus associated with the deficiency of *COUP-TFII*
519 suggested that the regulatory network related to *COUP-TF* genes during the early
520 morphogenesis of the hippocampus could be much more complicated than suspected and
521 should be investigated in our future study.
522
523 **4. *COUP-TF* genes are imperative for the formation of the trisynaptic circuit**
524 The hippocampus and entorhinal cortex (EC) are interconnected through various neural
525 circuits to mediate the flow of the information associated with declarative memory (Basu &
526 Siegelbaum, 2015). Both direct and indirect glutamatergic circuits are involved in the relay of
527 information from the EC to the hippocampal CA1, and the trisynaptic pathway is the most
528 well-characterized indirect circuit. The EC sends sensory signals from association cortices
529 via the perforant path to the DG, then the DG granule cells send excitatory mossy fiber
530 projections to CA3 pyramidal neurons, and CA3 pyramidal neurons project to CA1 via the
531 Schaffer collaterals (H. Lee, GoodSmith, & Knierim, 2020). Consistent with the high
532 expression of COUP-TFI in the dorsal hippocampus and COUP-TFII in the ventral
533 hippocampus (Figure 1), the dorsal trisynaptic circuit is specifically damaged in *COUP-TFI*
534 mutants, as is the ventral trisynaptic circuit in *COUP-TFII* mutant mice. Moreover, the

535 hippocampal trisynaptic circuit was almost completely absent in the double mutants (Figure 4,
536 and our unpublished observations). The information transfer associated with the trisynaptic
537 circuits should be abolished particularly in the dorsal and/or the ventral hippocampus in the
538 above corresponding genetic mouse models. Interestingly, *COUP-TFI* is also required to
539 specify the medial EC cell fate (J. Feng et al., 2021). Therefore, the impaired formation and
540 function of trisynaptic circuits could be caused by the abnormal development of CA1, CA3,
541 DG or EC lineages. Nonetheless, given that newborn granule neurons are continuously
542 generated in the adult DG to integrate into the existing neural circuits essential for declarative
543 memory (Toda, Parylak, Linker, & Gage, 2019; Tuncdemir, Lacefield, & Hen, 2019) and that
544 hippocampal adult neurogenesis was severely compromised in the *COUP-TF* double mutant
545 (Figure 3—figure supplement 1), we could not exclude the possibility that impaired adult
546 neurogenesis may also contribute to the malformation and impaired function of the
547 trisynaptic pathway in double mutants. We would like to investigate what sort of synaptic
548 circuitry is compromised either physiologically or morphologically in the trisynaptic circuit
549 of individual animal model in detail in future studies.
550
551 The hippocampus is heterogeneous along its dorsoventral axis, and either the dorsal or
552 ventral hippocampus generates unique and distinguishable characteristics of gene expression
553 and connectivity, which enable the hippocampus to execute an integrative function from the
554 encoding and retrieval of certain declarative memory to adaptive behaviors. Lesions of the
555 dorsal hippocampus, which are essential for the cognitive process of learning and memory,
556 lead to amnesia and ID; while damage to the ventral hippocampus, which is central for
557 emotion and affection, is highly associated with psychiatric disorders including depression,
558 anxiety, and schizophrenia. Our findings in this study reveal novel intrinsic mechanisms by
559 which two nuclear receptor genes, *COUP-TFI* and *-TFII*, which are associated with NDD or

CHD, converge to govern the differentiation and integration of the hippocampus along the dorsoventral axis morphologically and functionally. Furthermore, our present study provides novel genetic model systems to investigate the crosstalk among the hippocampal complex in gene expression, morphogenesis, cell fate specification and differentiation, connectivity, functions of learning/memory and emotion/anxiety, adaptive behaviors, and the etiology of neurological diseases. Nevertheless, many enigmas, such as whether and how the abnormalities of either the dorsal or ventral hippocampus affect the characteristics of the other, remain unsolved. In addition to the excitatory lineages and circuits, interneurons and inhibitory circuits play vital roles in maintaining the plasticity and functions of the hippocampus. We also wonder whether and how defects in interneurons and inhibitory circuits could contribute to the compromised morphogenesis, connectivity, and functions of the hippocampus and the etiology of psychiatric and neurological conditions including ID, ASD, depression, anxiety, and schizophrenia.

Materials and Methods

Animals

COUP-TFI-floxed mice, *COUP-TFII-floxed* mice, *Emx1*^{Cre} mice and *RX*^{Cre} mice (Swindell et al., 2006) (PMID: 16850473) used in the study were of the C57B6/129 mixed background. The noon of vaginal plug day was set as the embryonic day 0.5 (E0.5). Only male mice at age of 10 weeks or older were used in the Morris water maze. For other experiments, both male and female mice were used. All animal protocols were approved by the Institutional Animal Care and Use Committee (IACUC) at the Shanghai Institute of Biochemistry and Cell Biology, Chinese Academy of Sciences (Protocols: SIBCB-NAF-14-001-S308-001). All methods were performed in accordance with the relevant guidelines and regulations. Only the littermates were used for the comparison.

586 **Nissl staining**

587 We used xylene to dewax paraffin sections, followed by rinsing with 100%, 95%, and 70%
588 ethanol. The slides were stained in 0.1% Cresyl Violet solution for 25 mins. Then the
589 sections were washed quickly in the water and differentiated in 95% ethanol. We used 100%
590 ethanol to dehydrate the slides, followed by rinsing with the xylene solution. Finally, the
591 neutral resin medium was used to mount the slides.

592

593 **Immunohistochemical (IHC) staining**

594 The paraffin sections were dewaxed and rehydrated as described above for Nissl staining.
595 The slides were boiled in 1×antigen retrieval solution (DAKO) under microwave conditions
596 for 15 min. After cooled to room temperature (RT), the slides were incubated with 3% H_2O_2
597 for 30 min. Then, the slides were treated with blocking buffer for 60 min at RT and then
598 incubated with the primary antibody in the hybridization buffer (10×diluted blocking buffer)
599 overnight (O/N) at 4 °C. The next day, the tyramide signal amplification kit (TSA)
600 (Invitrogen) was used according to the manufacturer's protocol. After being incubated with
601 1%TSA blocking buffer, the sections were treated with a biotinylated secondary antibody for
602 60 min at RT. After being washed with 1×PBS three times, the slides were incubated with
603 1×HRP-conjugated streptavidin for 1 h. Next, the tyramide working solution was prepared,
604 including the 0.15‰ H_2O_2 in distilled water, the 100×diluted tyramide substrate solution
605 (tyramide-488 or tyramide-594), and the amplification buffer. The sections were incubated
606 with the working solution for 10 min. Then the slides were counterstained with DAPI and
607 mounted with the antifade mounting medium (Southern Biotech) (S. Feng et al., 2017; Zhang
608 et al., 2020). Finally, the sections were observed and images were captured with a digital
609 fluorescence microscope (Zeiss).

610 The following primary antibodies were used in the study: mouse anti-COUP-TFI (1:1000,
611 R&D, Cat # PP-H8132-00), mouse anti-COUP-TFII (1:2000, R&D, Cat # PP-H7147-00),
612 rabbit anti-COUP-TFII (1:2000, a gift from Dr. Zhenzhong Xu, Zhejiang University, China),
613 rabbit anti-HuB (1:500, Abcam, Cat # ab204991), rat anti-Ctip2 (1:500, Abcam, Cat #
614 ab18465), rabbit anti-Wfs1 (1:500, ProteinTech, Cat # 11558-1-AP), goat anti-Prox1 (1:500,
615 R&D, Cat # AF2727), rabbit anti-Calretinin (1:500, Sigma, Cat # C7479), rabbit anti-
616 Calbindin (1:500, Swant, Cat # CB38), mouse anti-SMI312 (1:200, Covance, Cat # SMI-
617 312R), rabbit anti-Sox2 (1:500, Affinity BioReagents, Cat # PA1-16968), rat anti-Tbr2
618 (1:500, Thermo Fisher, Cat # 12-4875-82), goat anti-NeuroD1 (1:200, Santa Cruz, Cat # sc-
619 1084), goat anti-Lhx2 (1:200, Santa Cruz, Cat # sc-19344), goat anti-Lhx5 (1:200, R&D, Cat
620 # AF6290), goat anti-β-galactosidase (LacZ) (1:400, Biogenesis, Cat # 4600-1409), mouse
621 anti-GFAP (1:500, Sigma, Cat # G3893), rabbit anti-Nestin (1:200, Santa Cruz, Cat # sc-
622 20978), goat anti-Dcx (1:500, Santa Cruz, Cat # sc-8066). The following secondary
623 antibodies were used in the study: donkey anti-mouse IgG biotin-conjugated (1:400,
624 JacksonImmuno, Cat # 715-065-150), donkey anti-rabbit IgG biotin-conjugated (1:400,
625 JacksonImmuno, Cat # 711-065-152), donkey anti-goat IgG biotin-conjugated (1:400,
626 JacksonImmuno, Cat # 705-066-147), donkey anti-rat IgG biotin-conjugated (1:400,
627 JacksonImmuno, Cat # 712-065-150).
628
629 **Western blotting**
630 We homogenized the isolated dorsal and ventral hippocampus tissues from 1-month-old mice
631 respectively in the RIPA buffer (Applygen) with protease inhibitor cocktail (Sigma) and
632 phosphatase inhibitors (Invitrogen) and then centrifuged at the speed of 12,000 rpm for 30
633 mins. We collected the supernatants and analyzed the total concentrations by the BCA kit
634 (Applygen). Gradient SDS-PAGE gels were used to separate the same amounts of protein

635 sample (40 μg/lane), and then the proteins were transferred to the PVDF membranes
636 (Millipore). After being blocked by the 3% BSA (Sigma) for 2h, the membranes that
637 contained proteins were incubated by primary antibodies at 4 °C O/N. The membranes were
638 rinsed with 1×PBST three times for 10 mins and then treated with biotinylated secondary
639 antibodies for 2h at RT. After washing with 1×PBST, membranes were treated with the HRP-
640 conjugated streptavidin for 1h at RT. Finally, we used the chemiluminescence detection
641 system (Tanon) to detect the bands. The density of the protein band was analyzed by the
642 software Image J.

643 The primary antibodies were used in the experiment as below: mouse anti-COUP-TFI
644 (1:2000, R&D, Cat # PP-H8132-00), rabbit anti-COUP-TFII (1:3000, a gift from Dr.
645 Zhenzhong Xu, Zhejiang University, China), mouse anti-GAPDH (1:1000, Santa Cruz, Cat #
646 sc-32233). The following secondary antibodies were applied in the study, including goat anti-
647 mouse IgG biotin-conjugated (1:1000, KPL, Cat # 16-18-06), goat anti-rabbit IgG biotin-
648 conjugated (1:1000, KPL, Cat # 16-15-06).

649

650 **Golgi staining**

651 Deep anesthesia was performed before sacrificing the control and mutant mice, and the brains
652 were immediately isolated. The FD rapid GolgiStain kit (FD NeuroTech) was used to process
653 the brain tissue samples, which were immersed in an equal volume of immersion solution
654 mixed with solutions A and B and stored in the dark for two weeks at RT. At least 5mL of
655 immersion solution was used for each cubic meter of the tissue. To achieve the best results,
656 the container of tissue was gently swirled from side to side twice a week during the
657 incubating period. Afterwards, the brain tissue was transferred to solution C in the dark at RT
658 for at least 72 hours (up to 1 week). Finally, the tissues were cut into 100 μm thick slices with
659 a cryostat at -20°C to -22°C and transferred to gelatin-coated microscope slides containing

660 solution C using a sample retriever. The slices were dried naturally at RT. The concrete
661 staining procedure of the kit was followed using the manufactory's protocol. Then, the
662 sections were rinsed twice with double-distilled water for 4 minutes each time. The slices
663 were placed in a mixture of one volume of solution D, one volume of solution E, and two
664 volumes of double distilled water for 10 minutes and were rinsed twice with distilled water
665 for 4 minutes each time. The sections were later dehydrated in 50%, 75%, and 95% ethanol
666 for 4 minutes respectively. Next, the slices were dehydrated in 100% ethanol 4 times for 4
667 minutes each time. Finally, the sections were cleared in xylene and mounted with a neutral
668 resin medium.
669
670 **Morris water maze**
671 By recording the time spent by the mice swimming in the water tank and finding the escape
672 platform hidden underwater, and the swimming trajectory, the Morris water maze test can
673 objectively reflect the spatial learning and memory ability of the mice. The test was divided
674 into the control and mutant group with at least eight mice in each group. We poured tap water
675 into the water maze tank and added an appropriate amount of well-mixed, milky white food
676 dye. The height of the liquid level was about 1 cm higher than the escape platform, and the
677 water temperature was kept at about 25±1℃. At the same time, four markers of different
678 shapes were pasted on the four directions of the inner wall above the water tank to distinguish
679 different directions. The Morris water maze test was divided into the training phase and the
680 probe trial phase. The training phase lasted for 6 days, 4 times a day, and the interval between
681 each training was about 30 minutes. During training, the mice were placed into the tank from
682 the entry points of four different quadrants facing the inner wall, and their latency was
683 recorded from the time they entered the water to the time they found a hidden underwater
684 platform and stood on it. After the mouse found the platform, we let it stay on the platform

for 10 seconds before removing it. If the mouse failed to discover the platform 60 seconds after entering the water, it was guided to find the platform and left to stay for 10 seconds. Each mouse was placed into the water tank from four water entry points and recorded as one training session. The probe trial was carried out on the seventh day, and the underwater platform was removed. Each experimental mouse was put into the water tank at the same water entry point and allowed to move for 60 seconds. The time that each mouse spent in the quadrant, where the platform was originally placed, was recorded.

RNA isolation and quantitative real-time PCR

Total RNAs were prepared from the whole telencephalon of the control (n=5) and double mutant (n=3) mice at E11.5 respectively, with the TRIzol Reagent (Invitrogen) by following the manufactory's protocol. Reverse-transcription PCR and real-time quantitative PCR assays were performed as described previously (Tang et al., 2012). A student's t-test was used to compare the means of the relative mRNA levels between the control group and mutant group. Primer sequences are as follows:

Axin2-f, 5'-*CTGCTGGTCAGGCAGGAG*-3', *Axin2-r*, 5'-*TGCCAGTTTCTTTGGCTCTT*-3'; *Coup-tfI-f*, 5'-*CAAAGCCATCGTGCTATTCA*-3', *Coup-tfI-r*, 5'-*CCTGCAGGCTTTCGATGT*-3'; *Coup-tfII-f*, 5'-*CCTCAAAGTGGGCATGAGAC*-3', *Coup-tfII-r*, 5'-*TGGGTAGGCTGGGTAGGAG*-3'; *Emx1-f*, 5'-*CTCTCCGAGACGCAGGTG*-3', *Emx1-r,* 5'-*CTCAGACTCCGGCCCTTC*-3'; *Emx2-f*, 5'-*CACGCTTTTGAGAAGAACCA*-3', *Emx2-r,* 5'-*GTTCTCCGGTTCTGAAACCA*-3'; *Foxg1-f*, 5'-*GAAGGCCTCCACAGAACG*-3', *Foxg1-r*, 5'-*GGCAAGGCATGTAGCAAAAG*-3'; *Gli3-f*, 5'-*TGATCCATCTCCTATTCCTCCA*-3', *Gli3-r*, 5'-*TCTGGATACGTCGGGCTACT*-3'; *Lef1-f*, 5'-*TCCTGAAATCCCCACCTTCT*-3', *Lef1-r*, 5'-*TGGGATAAACAGGCTGACCT*-3'; *Lhx2-f*, 5'-*CAGCTTGCGCAAAAGACC*-3', *Lhx2-r*, 5'-*TAAAAGGTTGCGCCTGAACT*-3'; *Lhx5-f*, 5'-*TGTGCAATAAGCAGCTATCCA*-3', *Lhx5-r,*

5’-*CAAACTGCGGTCCGTACA*-3’; *Otx1-f*, 5’-*CCAGAGTCCAGAGTCCAGGT*-3’, *Otx1-r*, 5’-*CCGGGTTTTCGTTCCATT*-3’; *Otx2-f*, 5’-*GGTATGGACTTGCTGCATCC*-3’, *Otx2-r*, 5’-*CGAGCTGTGCCCTAGTAAATG*-3’; *Pax6-f*, 5’-*GTTCCCTGTCCTGTGGACTC*-3’, *Pax6-r*, 5’-*ACCGCCCTTGGTTAAAGTCT*-3’; *Tcf4-f*, 5’-*AAATGGCCACTGCTTGATGT*-3’, *Tcf4-r*, 5’-*GCACCACCGGTACTTTGTTC*-3’.

Quantification and statistical analysis

The number of specified immunofluorescent marker-positive cells was assessed by Image J Cell Counter in full image fields. Three brain sections per mouse were counted for each index. GraphPad Prism 7.0 (GraphPad) was used to perform statistical analysis. The data analysis used one-way analysis of variance (ANOVA), Dunnett’s or Tukey’s post hoc tests, and student’s unpaired t-test. The data were expressed as the mean ± SEM. The data obtained from at least three independent replicates were used for statistical analysis. $P < 0.05$ was considered the significant statistical difference.

Acknowledgements

We thank Ms. Emerald Tang for her assistance with the manuscript. This work was supported by National Natural Science Foundation of China (31671508) and Guangdong Provincial Basic and Applied Basic Research Fund (2021A1515011299) to K.T; and in part by the National Key Basic Research and Development Program of China (2018YFA0108500, 2019YFA0801402, 2018YFA0800100, 2018YFA0108000, 2018YFA0107200, 2017YFA0102700), "Strategic Priority Research Program" of the Chinese Academy of Sciences, Grant No. (XDA16020501, XDA16020404) to N. J.

Data availability

Numerical data are available in the manuscript and supporting files.

Competing interests

The authors declare no competing interests.

References

Al Turki, S., Manickaraj, A. K., Mercer, C. L., Gerety, S. S., Hitz, M. P., Lindsay, S., . . . Hurles, M. E. (2014). Rare variants in NR2F2 cause congenital heart defects in humans. *Am J Hum Genet, 94*(4), 574-585. doi:10.1016/j.ajhg.2014.03.007

Alzu'bi, A., Lindsay, S. J., Harkin, L. F., McIntyre, J., Lisgo, S. N., & Clowry, G. J. (2017). The Transcription Factors COUP-TFI and COUP-TFII have Distinct Roles in Arealisation and GABAergic Interneuron Specification in the Early Human Fetal Telencephalon. *Cereb Cortex, 27*(10), 4971-4987. doi:10.1093/cercor/bhx185

Amaral, D. G. (1993). Emerging principles of intrinsic hippocampal organization. *Current Opinion in Neurobiology, 3*(2), 225-229. doi:https://doi.org/10.1016/0959-4388(93)90214-J

Anacker, C., & Hen, R. (2017). Adult hippocampal neurogenesis and cognitive flexibility - linking memory and mood. *Nat Rev Neurosci, 18*(6), 335-346. doi:10.1038/nrn.2017.45

Armentano, M., Chou, S. J., Tomassy, G. S., Leingärtner, A., O'Leary, D. D., & Studer, M. (2007). COUP-TFI regulates the balance of cortical patterning between frontal/motor and sensory areas. *Nat Neurosci, 10*(10), 1277-1286. doi:10.1038/nn1958

Baik, J. H. (2020). Stress and the dopaminergic reward system. *Exp Mol Med, 52*(12), 1879-1890. doi:10.1038/s12276-020-00532-4

Bast, T. (2007). Toward an integrative perspective on hippocampal function: from the rapid encoding of experience to adaptive behavior. *Rev Neurosci, 18*(3-4), 253-281. doi:10.1515/revneuro.2007.18.3-4.253

Basu, J., & Siegelbaum, S. A. (2015). The Corticohippocampal Circuit, Synaptic Plasticity, and Memory. *Cold Spring Harb Perspect Biol, 7*(11). doi:10.1101/cshperspect.a021733

Bertacchi, M., Romano, A. L., Loubat, A., Tran Mau-Them, F., Willems, M., Faivre, L., . . . Studer, M. (2020). NR2F1 regulates regional progenitor dynamics in the mouse neocortex and cortical gyrification in BBSOAS patients. *EMBO J, 39*(13), e104163. doi:10.15252/embj.2019104163

Bliss, T. V., & Lomo, T. (1973). Long-lasting potentiation of synaptic transmission in the dentate area of the anaesthetized rabbit following stimulation of the perforant path. *J Physiol, 232*(2), 331-356. doi:10.1113/jphysiol.1973.sp010273

Bosch, D. G., Boonstra, F. N., Gonzaga-Jauregui, C., Xu, M., de Ligt, J., Jhangiani, S., . . . Schaaf, C. P. (2014). NR2F1 mutations cause optic atrophy with intellectual disability. *Am J Hum Genet, 94*(2), 303-309. doi:10.1016/j.ajhg.2014.01.002

Bryant, K. G., & Barker, J. M. (2020). Arbitration of Approach-Avoidance Conflict by Ventral Hippocampus. *Front Neurosci, 14*, 615337. doi:10.3389/fnins.2020.615337

Cenquizca, L. A., & Swanson, L. W. (2007). Spatial organization of direct hippocampal field CA1 axonal projections to the rest of the cerebral cortex. *Brain Res Rev, 56*(1), 1-26. doi:10.1016/j.brainresrev.2007.05.002

Contesse, T., Ayrault, M., Mantegazza, M., Studer, M., & Deschaux, O. (2019). Hyperactive and anxiolytic-like behaviors result from loss of COUP-TFI/Nr2f1 in the mouse cortex. *Genes Brain Behav, 18*(7), e12556. doi:10.1111/gbb.12556

Del Pino, I., Tocco, C., Magrinelli, E., Marcantoni, A., Ferraguto, C., Tomagra, G., . . . Studer, M. (2020). COUP-TFI/Nr2f1 Orchestrates Intrinsic Neuronal Activity during Development of the Somatosensory Cortex. *Cereb Cortex, 30*(11), 5667-5685. doi:10.1093/cercor/bhaa137

Eichenbaum, H. (2017). On the Integration of Space, Time, and Memory. *Neuron, 95*(5), 1007-1018. doi:10.1016/j.neuron.2017.06.036

Eichenbaum, H., & Cohen, N. J. (2014). Can we reconcile the declarative memory and spatial navigation views on hippocampal function? *Neuron, 83*(4), 764-770. doi:10.1016/j.neuron.2014.07.032

Fanselow, M. S., & Dong, H. W. (2010). Are the dorsal and ventral hippocampus functionally distinct structures? *Neuron, 65*(1), 7-19. doi:10.1016/j.neuron.2009.11.031

Feng, J., Hsu, W. H., Patterson, D., Tseng, C. S., Hsing, H. W., Zhuang, Z. H., . . . Chou, S. J. (2021). COUP-TFI specifies the medial entorhinal cortex identity and induces differential cell adhesion to determine the integrity of its boundary with neocortex. *Sci Adv, 7*(27). doi:10.1126/sciadv.abf6808

Feng, S., Xing, C., Shen, T., Qiao, Y., Wang, R., Chen, J., . . . Tang, K. (2017). Abnormal Paraventricular Nucleus of Hypothalamus and Growth Retardation Associated with Loss of Nuclear Receptor Gene COUP-TFII. *Sci Rep, 7*(1), 5282. doi:10.1038/s41598-017-05682-6

Flore, G., Di Ruberto, G., Parisot, J., Sannino, S., Russo, F., Illingworth, E. A., . . . De Leonibus, E. (2017). Gradient COUP-TFI Expression Is Required for Functional Organization of the Hippocampal Septo-Temporal Longitudinal Axis. *Cereb Cortex, 27*(2), 1629-1643. doi:10.1093/cercor/bhv336

Galceran, J., Miyashita-Lin, E. M., Devaney, E., Rubenstein, J. L., & Grosschedl, R. (2000). Hippocampus development and generation of dentate gyrus granule cells is regulated by LEF1. *Development, 127*(3), 469-482. doi:10.1242/dev.127.3.469

Gao, X., Arlotta, P., Macklis, J. D., & Chen, J. (2007). Conditional knock-out of beta-catenin in postnatal-born dentate gyrus granule neurons results in dendritic malformation. *J Neurosci, 27*(52), 14317-14325. doi:10.1523/jneurosci.3206-07.2007

Gould, E., & Cameron, H. A. (1996). Regulation of neuronal birth, migration and death in the rat dentate gyrus. *Dev Neurosci, 18*(1-2), 22-35. doi:10.1159/000111392

Hebert, J. M., & Fishell, G. (2008). The genetics of early telencephalon patterning: some assembly required. *Nat Rev Neurosci, 9*(9), 678-685. doi:10.1038/nrn2463

Herman, J. P., McKlveen, J. M., Ghosal, S., Kopp, B., Wulsin, A., Makinson, R., . . . Myers, B. (2016). Regulation of the Hypothalamic-Pituitary-Adrenocortical Stress Response. *Compr Physiol, 6*(2), 603-621. doi:10.1002/cphy.c150015

High, F. A., Bhayani, P., Wilson, J. M., Bult, C. J., Donahoe, P. K., & Longoni, M. (2016). De novo frameshift mutation in COUP-TFII (NR2F2) in human congenital diaphragmatic hernia. *Am J Med Genet A, 170*(9), 2457-2461. doi:10.1002/ajmg.a.37830

Hoover, W. B., & Vertes, R. P. (2007). Anatomical analysis of afferent projections to the medial prefrontal cortex in the rat. *Brain Struct Funct, 212*(2), 149-179. doi:10.1007/s00429-007-0150-4

Kandel, E. R., Dudai, Y., & Mayford, M. R. (2014). The molecular and systems biology of memory. *Cell, 157*(1), 163-186. doi:10.1016/j.cell.2014.03.001

Kim, B. J., Takamoto, N., Yan, J., Tsai, S. Y., & Tsai, M. J. (2009). Chicken Ovalbumin Upstream Promoter-Transcription Factor II (COUP-TFII) regulates growth and patterning of the postnatal mouse cerebellum. *Dev Biol, 326*(2), 378-391. doi:10.1016/j.ydbio.2008.11.001

Kishi, T., Tsumori, T., Ono, K., Yokota, S., Ishino, H., & Yasui, Y. (2000). Topographical organization of projections from the subiculum to the hypothalamus in the rat. *J Comp Neurol, 419*(2), 205-222. doi:10.1002/(sici)1096-9861(20000403)419:2<205::aid-cne5>3.0.co;2-0

Lee, H., GoodSmith, D., & Knierim, J. J. (2020). Parallel processing streams in the hippocampus. *Curr Opin Neurobiol, 64*, 127-134. doi:10.1016/j.conb.2020.03.004

Lee, S. M., Tole, S., Grove, E., & McMahon, A. P. (2000). A local Wnt-3a signal is required for development of the mammalian hippocampus. *Development, 127*(3), 457-467. doi:10.1242/dev.127.3.457

Leid, M., Ishmael, J. E., Avram, D., Shepherd, D., Fraulob, V., & Dolle, P. (2004). CTIP1 and CTIP2 are differentially expressed during mouse embryogenesis. *Gene Expr Patterns, 4*(6), 733-739. doi:10.1016/j.modgep.2004.03.009

Li, J., Sun, L., Peng, X. L., Yu, X. M., Qi, S. J., Lu, Z. J., . . . Shen, Q. (2021). Integrative genomic analysis of early neurogenesis reveals a temporal genetic program for differentiation and specification of preplate and Cajal-Retzius neurons. *PLoS Genet, 17*(3), e1009355. doi:10.1371/journal.pgen.1009355

Lisman, J., Buzsaki, G., Eichenbaum, H., Nadel, L., Ranganath, C., & Redish, A. D. (2017). Viewpoints: how the hippocampus contributes to memory, navigation and cognition. *Nat Neurosci, 20*(11), 1434-1447. doi:10.1038/nn.4661

Lodato, S., Tomassy, G. S., De Leonibus, E., Uzcategui, Y. G., Andolfi, G., Armentano, M., . . . Studer, M. (2011). Loss of COUP-TFI alters the balance between caudal ganglionic eminence- and medial ganglionic eminence-derived cortical interneurons and results in resistance to epilepsy. *J Neurosci, 31*(12), 4650-4662. doi:10.1523/jneurosci.6580-10.2011

Mangale, V. S., Hirokawa, K. E., Satyaki, P. R., Gokulchandran, N., Chikbire, S., Subramanian, L., . . . Monuki, E. S. (2008). Lhx2 selector activity specifies cortical identity and suppresses hippocampal organizer fate. *Science, 319*(5861), 304-309. doi:10.1126/science.1151695

Miquelajáuregui, A., Varela-Echavarría, A., Ceci, M. L., García-Moreno, F., Ricaño, I., Hoang, K., . . . Zhao, Y. (2010). LIM-homeobox gene Lhx5 is required for normal development of Cajal-Retzius cells. *J Neurosci, 30*(31), 10551-10562. doi:10.1523/jneurosci.5563-09.2010

Monuki, E. S., Porter, F. D., & Walsh, C. A. (2001). Patterning of the dorsal telencephalon and cerebral cortex by a roof plate-Lhx2 pathway. *Neuron, 32*(4), 591-604. doi:10.1016/s0896-6273(01)00504-9

Moore, S. A., & Iulianella, A. (2021). Development of the mammalian cortical hem and its derivatives: the choroid plexus, Cajal-Retzius cells and hippocampus. *Open Biol, 11*(5), 210042. doi:10.1098/rsob.210042

Moser, M. B., & Moser, E. I. (1998). Functional differentiation in the hippocampus. *Hippocampus, 8*(6), 608-619. doi:10.1002/(SICI)1098-1063(1998)8:6<608::AID-HIPO3>3.0.CO;2-7

O'Keefe, J., & Conway, D. H. (1978). Hippocampal place units in the freely moving rat: why they fire where they fire. *Exp Brain Res, 31*(4), 573-590. doi:10.1007/BF00239813

O'Keefe, J., & Dostrovsky, J. (1971). The hippocampus as a spatial map. Preliminary evidence from unit activity in the freely-moving rat. *Brain Res, 34*(1), 171-175. doi:10.1016/0006-8993(71)90358-1

O'Leary, O. F., & Cryan, J. F. (2014). A ventral view on antidepressant action: roles for adult hippocampal neurogenesis along the dorsoventral axis. *Trends Pharmacol Sci, 35*(12), 675-687. doi:10.1016/j.tips.2014.09.011

Penfield, W., & Milner, B. (1958). Memory deficit produced by bilateral lesions in the hippocampal zone. *AMA Arch Neurol Psychiatry, 79*(5), 475-497. doi:10.1001/archneurpsyc.1958.02340050003001

Pitkanen, A., Pikkarainen, M., Nurminen, N., & Ylinen, A. (2000). Reciprocal connections between the amygdala and the hippocampal formation, perirhinal cortex, and postrhinal cortex in rat. A review. *Ann N Y Acad Sci, 911*, 369-391. doi:10.1111/j.1749-6632.2000.tb06738.x

Porter, F. D., Drago, J., Xu, Y., Cheema, S. S., Wassif, C., Huang, S. P., . . . Westphal, H. (1997). Lhx2, a LIM homeobox gene, is required for eye, forebrain, and definitive erythrocyte development. *Development, 124*(15), 2935-2944. doi:10.1242/dev.124.15.2935

Roberts, A. C., Tomic, D. L., Parkinson, C. H., Roeling, T. A., Cutter, D. J., Robbins, T. W., & Everitt, B. J. (2007). Forebrain connectivity of the prefrontal cortex in the marmoset monkey (Callithrix jacchus): an anterograde and retrograde tract-tracing study. *J Comp Neurol, 502*(1), 86-112. doi:10.1002/cne.21300

Roy, A., Gonzalez-Gomez, M., Pierani, A., Meyer, G., & Tole, S. (2014). Lhx2 regulates the development of the forebrain hem system. *Cereb Cortex, 24*(5), 1361-1372. doi:10.1093/cercor/bhs421

Schuurmans, C., & Guillemot, F. (2002). Molecular mechanisms underlying cell fate specification in the developing telencephalon. *Curr Opin Neurobiol, 12*(1), 26-34. doi:10.1016/s0959-4388(02)00286-6

Scoville, W. B., & Milner, B. (1957). Loss of recent memory after bilateral hippocampal lesions. *J Neurol Neurosurg Psychiatry, 20*(1), 11-21. doi:10.1136/jnnp.20.1.11

Simeone, A., Gulisano, M., Acampora, D., Stornaiuolo, A., Rambaldi, M., & Boncinelli, E. (1992). Two vertebrate homeobox genes related to the Drosophila empty spiracles gene are expressed in the embryonic cerebral cortex. *EMBO J, 11*(7), 2541-2550. doi:10.1002/j.1460-2075.1992.tb05319.x

Strange, B. A., Witter, M. P., Lein, E. S., & Moser, E. I. (2014). Functional organization of the hippocampal longitudinal axis. *Nat Rev Neurosci, 15*(10), 655-669. doi:10.1038/nrn3785

Sugiyama, T., Osumi, N., & Katsuyama, Y. (2014). A novel cell migratory zone in the developing hippocampal formation. *J Comp Neurol, 522*(15), 3520-3538. doi:10.1002/cne.23621

Swindell, E. C., Bailey, T. J., Loosli, F., Liu, C., Amaya-Manzanares, F., Mahon, K. A., . . . Jamrich, M. (2006). Rx-Cre, a tool for inactivation of gene expression in the developing retina. *Genesis, 44*(8), 361-363. doi:10.1002/dvg.20225

Takeda, K., Inoue, H., Tanizawa, Y., Matsuzaki, Y., Oba, J., Watanabe, Y., . . . Oka, Y. (2001). WFS1 (Wolfram syndrome 1) gene product: predominant subcellular localization to endoplasmic reticulum in cultured cells and neuronal expression in rat brain. *Hum Mol Genet, 10*(5), 477-484. doi:10.1093/hmg/10.5.477

Tang, K., Rubenstein, J. L., Tsai, S. Y., & Tsai, M. J. (2012). COUP-TFII controls amygdala patterning by regulating neuropilin expression. *Development, 139*(9), 1630-1639. doi:10.1242/dev.075564

Toda, T., Parylak, S. L., Linker, S. B., & Gage, F. H. (2019). The role of adult hippocampal neurogenesis in brain health and disease. *Mol Psychiatry, 24*(1), 67-87. doi:10.1038/s41380-018-0036-2

Tole, S., Goudreau, G., Assimacopoulos, S., & Grove, E. A. (2000). Emx2 is required for growth of the hippocampus but not for hippocampal field specification. *J Neurosci, 20*(7), 2618-2625. Retrieved from https://www.ncbi.nlm.nih.gov/pubmed/10729342

Tuncdemir, S. N., Lacefield, C. O., & Hen, R. (2019). Contributions of adult neurogenesis to dentate gyrus network activity and computations. *Behav Brain Res, 374*, 112112. doi:10.1016/j.bbr.2019.112112

Tyng, C. M., Amin, H. U., Saad, M. N. M., & Malik, A. S. (2017). The Influences of Emotion on Learning and Memory. *Front Psychol, 8*, 1454. doi:10.3389/fpsyg.2017.01454

Vorhees, C. V., & Williams, M. T. (2006). Morris water maze: procedures for assessing spatial and related forms of learning and memory. *Nat Protoc, 1*(2), 848-858. doi:10.1038/nprot.2006.116

Yang, X., Feng, S., & Tang, K. (2017). COUP-TF Genes, Human Diseases, and the Development of the Central Nervous System in Murine Models. *Curr Top Dev Biol, 125*, 275-301. doi:10.1016/bs.ctdb.2016.12.002

Yoshida, M., Suda, Y., Matsuo, I., Miyamoto, N., Takeda, N., Kuratani, S., & Aizawa, S. (1997). Emx1 and Emx2 functions in development of dorsal telencephalon. *Development, 124*(1), 101-111. doi:10.1242/dev.124.1.101

Yu, D. X., Marchetto, M. C., & Gage, F. H. (2014). How to make a hippocampal dentate gyrus granule neuron. *Development, 141*(12), 2366-2375. doi:10.1242/dev.096776

Zhang, K., Yu, F., Zhu, J., Han, S., Chen, J., Wu, X., . . . Tang, K. (2020). Imbalance of Excitatory/Inhibitory Neuron Differentiation in Neurodevelopmental Disorders with an NR2F1 Point Mutation. *Cell Rep, 31*(3), 107521. doi:10.1016/j.celrep.2020.03.085

Zhao, Y., Sheng, H. Z., Amini, R., Grinberg, A., Lee, E., Huang, S., . . . Westphal, H. (1999). Control of hippocampal morphogenesis and neuronal differentiation by the LIM homeobox gene Lhx5. *Science, 284*(5417), 1155-1158. doi:10.1126/science.284.5417.1155

Zhou, C., Qiu, Y., Pereira, F. A., Crair, M. C., Tsai, S. Y., & Tsai, M. J. (1999). The nuclear orphan receptor COUP-TFI is required for differentiation of subplate neurons and guidance of thalamocortical axons. *Neuron, 24*(4), 847-859. doi:10.1016/s0896-6273(00)81032-6

Zhou, C., Tsai, S. Y., & Tsai, M. J. (2001). COUP-TFI: an intrinsic factor for early regionalization of the neocortex. *Genes Dev, 15*(16), 2054-2059. doi:10.1101/gad.913601

Zhou, X., Liu, F., Tian, M., Xu, Z., Liang, Q., Wang, C., . . . Yang, Z. (2015). Transcription factors COUP-TFI and COUP-TFII are required for the production of granule cells in the mouse olfactory bulb. *Development, 142*(9), 1593-1605. doi:10.1242/dev.115279

967 **Figure legends**

968

969 **Figure 1. Duplicated CA1 and CA3 domains are generated in the ventral hippocampus**

970 **of *RX*$^{Cre/+}$; *COUP-TFII*$^{F/F}$ mutant mice.**

971 **A,** The expression of COUP-TFI (**a, d, g, j, m**) and COUP-TFII (**b, e, h, k, n**) in coronal

972 sections (**a-f**) and sagittal sections (**g-o**) of the hippocampus at postnatal month 1 (1M);

973 representative Western blots and quantitative densitometry data for the expression of COUP-

974 TFI and COUP-TFII in the dorsal and ventral hippocampus at 1M (**p-q**). **B,** In coronal

975 sections along the rostrocaudal axis (**a-f**) and sagittal sections along the lateral-medial axis

976 (**g-l**) of the hippocampus in mutant mice, compared with that in control mice (**a-c**, **g-i**), the

977 ectopic CA-like structure, indicated by the star, was observed in the ventral region in *COUP-*

978 *TFII* gene mutant (*RX*$^{Cre/+}$; *COUP-TFII*$^{F/F}$) mice at 1M (**d-f**, **j-l**). **C,** The expression of HuB

979 and Ctip2 in the corresponding inserted area in **a-f** under a high magnification objective lens

980 at 1M (**g-r**); compared with those of control mice (**a-c**, **g-i**, **m-o**), the duplicated HuB-positive

981 CA3 domain, indicated by the star, and Ctip2-positive domains, indicated by the arrowhead,

982 were specifically observed in the ventral hippocampus (**d-f, p-r**) but not in the dorsal

983 hippocampus (**d-f**, **j-l**) of *COUP-TFII* mutant mice at 1M; Ctip2 positive AHi and MePD

984 amygdaloid nuclei were barely observed in the *COUP-TFII* mutant mice, indicated by the

985 arrows, instead of the ectopic CA domains at the prospective amygdaloid regions (**e-f**, **q-r**).

986 Data are expressed as the mean ± SEM. *Student's t test*, $^{*}P<0.05$, $^{**}P<0.01$. AHi,

987 amygdalohippocampal area; AMY, amygdala nuclei; CTX, cortex; dCA1, dorsal CA1; dCA3,

988 dorsal CA3; dDG, dorsal dentate gyrus; dHPC, dorsal hippocampus; MePD, posterodorsal

989 part of the medial amygdaloid nucleus; PMCo, posteromedial cortical amygdaloid nucleus;

990 vCA1, ventral CA1; vCA3, ventral CA3; vDG, ventral dentate gyrus; vHPC, ventral

991 hippocampus. Scale bars, **Aa-c**, **Ad-f**, **Aj-o**, **Cg-r**, 100 μm; **Ag-i**, **Ba-l, Ca-f**, 200μm.

992

993 **Figure 1—figure supplement 1. The expression of *COUP-TF* genes in the early**
994 **developing hippocampus and different conditional knock mouse models.**
995 **A,** The expression of *COUP-TFI* and *COUP-TFII* genes in the forebrain at E10.5 (**a-b**) and
996 E11.5 (**c-d**). **B,** The expression of *COUP-TFI* and *COUP-TFII* genes in the developing
997 hippocampus at E12.5 (**a-c**), E14.5 (**d-f**), and P0 (**g-l**). **C,** Compared with that of control mice
998 (**a-c**), *COUP-TFII* is efficiently deleted by RXCre recombinase in the hippocampus of
999 *COUP-TFII* mutant mice at 1M (**d-f**); *COUP-TFI* is clearly deleted by RXCre recombinase
1000 in the hippocampus of *COUP-TFI* mutant mice at 1M (**g-i**). Compared with that of control
1001 mice (**j-l**), COUP-TFI and -TFII were efficiently deleted by RXCre recombinase at the
1002 hippocampal primordium, including the MP and CH, in *COUP-TFI/-TFII* double-mutant
1003 mice at E14.5 (**m-o**). **D,** Compared with that of the control mice (**a-c, g-h**), the expression of
1004 *COUP-TFII* was significantly decreased in the hippocampal primordium of the homozygous
1005 mutant mice at E11.5; meanwhile, the LacZ signals obviously increased in the *COUP-TFII*
1006 homozygous mutant mice at E11.5 (**d-f, j-k**). Compared with that of the control mice (**i**), the
1007 expression of COUP-TFI is activated in the caudal hippocampal primordium of the
1008 homozygous mutant mice at E11.5 (**l**). CH, cortical hem; dHPC, dorsal hippocampus; HP,
1009 hippocampal primordium; HPC, hippocampus; MP, medial pallium; vHPC, ventral
1010 hippocampus. Scale bars, **Aa-d**, **Ba-f**, **Cj-o**, 200 μm; **Bg-l**, **Ca-i**, **Dg-l**, 100 μm; **Da-f**, 250 μm.
1011

1012 **Figure 2. The specification and differentiation of the dorsal CA1 lineage failed with the**
1013 **dysplastic dorsal hippocampus in *RX*$^{Cre/+}$; *COUP-TFI*$^{F/F}$ mutant mice.**
1014 **A,** In coronal sections along the rostrocaudal axis (**a-f**) and sagittal sections along the lateral-
1015 medial axis (**g-l**) of the hippocampus, compared with that of control mice (**a-c**, **g-i**), the dorsal
1016 hippocampus was shrunken, indicated by the star, in *COUP-TFI* gene mutant (*RX*$^{Cre/+}$;
1017 *COUP-TFI*$^{F/F}$) mice at 1M (**d-f**, **j-l**). **B,** The expression of HuB and Ctip2 in the

1018 corresponding inserted area in **a-f** under a high magnification objective lens at 1M (**g-r**);
1019 compared with that of control mice (**a-c**, **g-i**, **m-o**), the HuB-positive CA3 domain was
1020 reduced in the dorsal hippocampus, especially the Ctip2-positive dorsal CA1, which was
1021 barely detected in *COUP-TFI* mutant mice at 1M (**d-f**, **j-l**), while their expression in the
1022 ventral hippocampus was comparable between the controls and mutants (**d-f**, **p-r**). **C,** The
1023 expression of HuB and Wfs1 in the corresponding inserted area in **a-f** under a high
1024 magnification objective lens at 1M (**g-r**); the expression of HuB and the dCA1 marker Wfs1
1025 in the control (**a-c**, **g-i**, **m-o**) and *COUP-TFII* mutant mice (**d-f**, **j-l**, **p-r**) at 1M. Wfs1-positive
1026 dorsal CA1 could not be detected in *COUP-TFI* mutant mice at 1M, as indicated by the
1027 arrowhead. dHPC, dorsal hippocampus; HPC, hippocampus; vHPC, ventral hippocampus.
1028 Scale bars, **Aa-l**, **Ba-f**, **Ca-f,** 200 μm; **Bg-r**, **Cg-r,** 100 μm.
1029

1030 **Figure 2—figure supplement 1. Defects in *Emx1*$^{Cre/+}$; *COUP-TFI*$^{F/F}$ mutant mice.**
1031 **A,** Immunofluorescence staining data showed that compared with those of control mice (**a, c,**
1032 **e, g**), the proportions of either the Wfs1- or Ctip2-positive dorsal CA1 domain were reduced
1033 in *Emx1*$^{Cre/+}$; *COUP-TFI*$^{F/F}$ mutant mice at 3M (**b, d, f, h**). **B,** Golgi staining showed that
1034 compared with those of controls, the numbers of branch points and secondary dendrites of
1035 both apical and basal dendrites were significantly reduced in the dorsal hippocampal CA1
1036 pyramidal neurons of *Emx1*$^{Cre/+}$; *COUP-TFI*$^{F/F}$ mutant mice (**a-c**). **C,** The Morris water maze
1037 behavior test showed that compared with that of controls, spatial learning and memory were
1038 significantly damaged in *Emx1*$^{Cre/+}$; *COUP-TFI*$^{F/F}$ mutant mice. Data are expressed as the
1039 mean ± SEM. *Student's t test*, $^{*}P<0.05$, $^{**}P<0.01$, $^{***}P<0.001$. Scale bars, **Aa-h,** 100 μm; **Ba-**
1040 **b,** 50 μm.
1041

1042 **Figure 3. Defects in the hippocampus in *RX*$^{Cre/+}$; *COUP-TFI*$^{F/F}$; *COUP-TFII*$^{F/F}$ double-**
1043 **gene mutant mice.**
1044 **A,** In coronal sections along the rostrocaudal axis, compared with control mice (**a-d**), the
1045 hippocampus was atrophic in *RX*$^{Cre/+}$; *COUP-TFI*$^{F/F}$; *COUP-TFII*$^{F/F}$ double mutant mice,
1046 indicated by the star, and an ectopic unknown nucleus was observed in the caudal plates,
1047 indicated by the arrowhead (**e-h**). **B,** Compared with that of control mice (**a-c**, **g-i**), the
1048 expression of HuB, Ctip2, and Prox1 was decreased in the hippocampus of *COUP-TFI/-TFII*
1049 double-gene mutant mice at 3 weeks postnatal (3W) (**d-f**, **j-l**). **C,** Compared with that of
1050 control mice (**a-c**, **g-i**), the expression of HuB could not be detected in the presumptive CA3
1051 domain, and the expression of Ctip2 or Prox1 could not be detected in the presumptive DG
1052 domain of the prospective ventral hippocampus of *RX*$^{Cre/+}$; *COUP-TFI*$^{F/F}$; *COUP-TFII*$^{F/F}$
1053 double mutant mice. Scale bars, **Aa-h**, 200 μm; **Ba-l**, **Ca-l,** 100 μm.
1054
1055 **Figure 3—figure supplement 1. Adult neurogenesis was abnormal in the hippocampi of**
1056 ***COUP-TFI/-TFII* double-gene mutant mice.**
1057 **A,** The expression of GFAP and Nestin, markers of NSCs, in the SGZ of the vDG in control
1058 and *COUP-TFII* mutant mice at 1M (**a-h**), in the SGZ of the dDG in control and *COUP-TFI*
1059 mutant mice at 1M (**i-p**) and in the SGZ of the DG in control and *COUP-TFI/-TFII* double-
1060 gene mutant mice at 3W (**q-x**). **B**, The expression of Dcx, a marker of newborn neurons, in
1061 the SGZ of the vDG in control and *COUP-TFII* mutant mice at 1M (**a-d**), in the SGZ of the
1062 dDG in control and *COUP-TFI* mutant mice at 1M (**e-h**) and in the SGZ of the DG in control
1063 and *COUP-TFI/-TFII* double-gene mutant mice at 3W (**i-l**). **C,** Quantitative analysis of
1064 GFAP/Nestin-positive cells (**a**) and Dcx-positive cells (**b**) in the SGZ of the DG in control
1065 and *COUP-TFI/-TFII* double-gene mutant mice at 3W. The numbers of GFAP and Nestin
1066 double-positive NSCs and Dcx-positive newborn neurons were significantly reduced in

1067 double-mutant mice. Data are expressed as the mean ± SEM. *Student's t test*, $^{**}P<0.01$,
1068 $^{***}P<0.001$. dDG, dorsal DG; NSC, neural stem cell; SGZ, subgranular zone; vDG, ventral
1069 DG. Scale bars, **Aa-x**, 50 μm; **Ba-l**, 100 μm.
1070
1071 **Figure 4. The impairment of hippocampal trisynaptic connectivity in *COUP-TFII***
1072 **single-gene, *COUP-TFI* single-gene, and *COUP-TFI/-TFII* double-gene mutant mice.**
1073 **A,** The expression of Calretinin, Calbindin, and SMI312 in the ventral hippocampus of the
1074 control (**a-b**, **e-f**, **i-j**) and *COUP-TFII* single-gene mutant mice (**c-d**, **g-h**, **k-l**). **B,** The
1075 expression of Calretinin, Calbindin, and SMI312 in the dorsal hippocampus of the control (**a-**
1076 **b**, **e-f**, **i-j**) and *COUP-TFI* single-gene mutant mice (**c-d**, **g-h**, **k-l**). **C,** The expression of
1077 Calretinin, Calbindin, and SMI312 in the hippocampus of the control (**a-b**, **e-f**, **i-j**) and
1078 *COUP-TFI*/*-TFII* double-gene mutant mice (**c-d**, **g-h**, **k-l**). dHPC, dorsal hippocampus; HPC,
1079 hippocampus; vHPC, ventral hippocampus. Scale bars, **Aa-l**, **Ba-l**, **Ca-l**, 100 μm.
1080
1081 **Figure 5. *COUP-TF* genes regulate the expression of key genes associated with early**
1082 **hippocampal development.**
1083 **A,** The expression profiles of genes involved in hippocampal development in control and the
1084 double mutant mice at E11.5. **B,** Compared with that of control mice (**a-b**, **a'-b', a''-b'', i-j,**
1085 **i'-j', q-r, q'-r'**), the expression of Lhx5 was reduced in double-mutant mice at E11.5 (**c-d**,
1086 **c'-d', c''-d''**), E13.5 (**k-l**, **k'-l'**) and E14.5 (**s-t**, **s'-t'**); the expression of Lhx2 was
1087 comparable between the control and double-mutant mice at E11.5 (**e-h**, **e'-h'**); and compared
1088 with that of control mice (**m-n**, **m'-n'**, **u-v**, **u'-v'**), the expression of Lhx2 was increased in
1089 double-mutant mice at E13.5 (**o-p**, **o'-p'**) and E14.5 (**w-x**, **w'-x'**). **C,** Compared with that of
1090 control mice (**a-b**, **a'-b'**), the expression of Sox2 was normal in double-mutant mice at E14.5
1091 (**c-d**, **c'-d'**); compared with that of control mice (**e-f**, **e'-f'**), the expression of Tbr2 was

1092 decreased in *COUP-TF* mutant mice at E14.5 (**g-h**, **g'-h'**); compared with that of control
1093 mice (**i-j**, **i'-j'**), the expression of NeuroD1 was reduced in double-mutant mice at E14.5 (**k-l**,
1094 **k'-l'**). **D,** Quantitative analysis of Tbr2-positive cells and NeuroD1-positive cells in **Ce'-h'**
1095 and **Ci'-l'**. **E,** In the hippocampal primordium of the early embryo, *COUP-TFI* is expressed
1096 dorsally in the MP, and *COUP-TFII* is expressed ventrally in the CH. In the mature
1097 hippocampus, the expression of *COUP-TFI* is higher in the dorsal hippocampus, which is
1098 related to spatial learning and memory, and the expression of *COUP-TFII* is mainly in the
1099 ventral hippocampus, which is associated with emotion and anxiety (**a**). Our findings support
1100 a novel molecular mechanism by which *COUP-TFI* and *COUP-TFII* may cooperate to ensure
1101 the appropriate morphogenesis and functions of the hippocampus by modulating the *Lhx5-*
1102 *Lhx2* axis (**b**). Data are expressed as the mean ± SEM. *Student's t test*, $^{**}P<0.01$. CH, cortical
1103 hem; ChP, choroid plexus; DP, dorsal pallium; HP, hippocampal primordium; MP, medial
1104 pallium. Scale bars, **Ba-x, Ca-l**, 200 μm.

1105

1106 **Figure 5—figure supplement 1. *COUP-TFI* and *-TFII* genes coordinate to control**
1107 **distinct characteristics of the hippocampus.**

1108 Roles of *COUP-TFI* and *COUP-TFII* genes in the development and function of the
1109 hippocampus and the association with neurological diseases. *COUP-TFI* is required for the
1110 morphogenesis of the dorsal hippocampus and the specification of dorsal CA1 pyramidal
1111 neuron lineage, which are associated with neurodevelopmental disorders, including ID and
1112 ASD. *COUP-TFII* is required to prevent the duplication of the CA1 and CA3 lineages of the
1113 ventral hippocampus, which may be related to psychiatric diseases such as depression,
1114 anxiety, or schizophrenia. The *COUP-TFI* and *COUP-TFII* genes are novel intrinsic
1115 regulatory genes, which cooperate with each other to ensure the early morphogenesis of the
1116 hippocampus.

1117

1118

1119

1120 **The information of the source data files**

1121 **Figure 1-source data 1.** The Nissl staining results of the control and *RX*$^{Cre/+}$; *COUP-TFII*$^{F/F}$

1122 mutant mice at 1M (part 1); the expression of HuB and Ctip2 in the hippocampus of the

1123 control and *RX*$^{Cre/+}$; *COUP-TFII*$^{F/F}$ mutant mice at 1M (part 1).

1124

1125 **Figure 1-source data 2.** The expression of COUP-TFI and COUP-TFII in coronal sections

1126 and sagittal sections of the mouse brain at 1M (part 1); the expression of HuB and Ctip2 in

1127 the hippocampus of the control and *RX*$^{Cre/+}$; *COUP-TFII*$^{F/F}$ mutant mice at 1M (part 2).

1128

1129 **Figure 1-source data 3.** The expression of COUP-TFI and COUP-TFII in coronal sections

1130 and sagittal sections of the mouse brain at 1M (part 2).

1131

1132 **Figure 1-source data 4.** The expression of COUP-TFI and COUP-TFII in sagittal sections of

1133 the mouse brain at 1M (part 1).

1134

1135 **Figure 1-source data 5.** The expression of COUP-TFI and COUP-TFII in sagittal sections of

1136 the mouse brain at 1M (part 2); the Nissl staining results of the control and *RX*$^{Cre/+}$; *COUP-*

1137 *TFII*$^{F/F}$ mutant mice at 1M (part 2).

1138

1139 **Figure 1-source data 6.** The expression of COUP-TFI and COUP-TFII in sagittal sections of

1140 the mouse brain at 1M (part 3); Western blots data for the expression of COUP-TFI and

1141 COUP-TFII in the dorsal and ventral hippocampus at 1M; the Nissl staining results of the

1142 control and *RX*$^{Cre/+}$; *COUP-TFII*$^{F/F}$ mutant mice at 1M (part 3).

1143

1144 **Figure 1-figure supplement 1-source data 1.** The expression of *COUP-TFI* and *COUP-*
1145 *TFII* genes in the developing hippocampus at E12.5; the deletion efficiency of RXCre
1146 recombinase in the hippocampus of $RX^{Cre/+}$; $COUP\text{-}TFII^{F/F}$, $RX^{Cre/+}$; $COUP\text{-}TFI^{F/F}$, and
1147 $RX^{Cre/+}$; $COUP\text{-}TFI^{F/F}$; $COUP\text{-}TFII^{F/F}$ mice (part 1).

1148

1149 **Figure 1-figure supplement 1-source data 2.** The expression of *COUP-TFI* and *COUP-*
1150 *TFII* genes in the telencephalon at E10.5, E11.5, E14.5, and P0; the deletion efficiency of
1151 RXCre recombinase in the hippocampus of $RX^{Cre/+}$; $COUP\text{-}TFII^{F/F}$, $RX^{Cre/+}$; $COUP\text{-}TFI^{F/F}$,
1152 and $RX^{Cre/+}$; $COUP\text{-}TFI^{F/F}$; $COUP\text{-}TFII^{F/F}$ mice (part 2).

1153

1154 **Figure 2-source data 1.** The Nissl staining results of the control and $RX^{Cre/+}$; $COUP\text{-}TFI^{F/F}$
1155 mutant mice at 1M (part 1).

1156

1157 **Figure 2-source data 2.** The Nissl staining results of the control and $RX^{Cre/+}$; $COUP\text{-}TFI^{F/F}$
1158 mutant mice at 1M (part 2); the expression of HuB and Wfs1 in the hippocampus of the
1159 control and $RX^{Cre/+}$; $COUP\text{-}TFI^{F/F}$ mutant mice at 1M.

1160

1161 **Figure 2-source data 3.** The expression of HuB and Ctip2 in the hippocampus of the control
1162 and $RX^{Cre/+}$; $COUP\text{-}TFI^{F/F}$ mutant mice at 1M.

1163

1164 **Figure 2-source data 4.** The expression of HuB, Wfs1, and Ctip2 in the hippocampus of the
1165 control and $RX^{Cre/+}$; $COUP\text{-}TFI^{F/F}$ mutant mice at 1M.

1166

1167 **Figure 2-figure supplement 1-source data 1.** The expression of Wfs1 and Ctip2 in the
1168 dorsal hippocampus of the control and *Emx1*$^{Cre/+}$; *COUP-TFI*$^{F/F}$ mutant mice at 3M; Golgi
1169 staining results of the dorsal hippocampal CA1 pyramidal neurons and Morris water maze
1170 behavior test data of the control and *Emx1*$^{Cre/+}$; *COUP-TFI*$^{F/F}$ mutant mice.
1171
1172 **Figure 3-source data 1.** The Nissl staining results of the control and *RX*$^{Cre/+}$; *COUP-TFI*$^{F/F}$;
1173 *COUP-TFII*$^{F/F}$ double-gene mutant mice at 3W.
1174
1175 **Figure 3-source data 2.** The expression of HuB and Ctip2 in the hippocampus of the control
1176 and *RX*$^{Cre/+}$; *COUP-TFI*$^{F/F}$; *COUP-TFII*$^{F/F}$ double-gene mutant mice at 3W.
1177
1178 **Figure 3-source data 3.** The expression of HuB and Prox1 in the hippocampus of the control
1179 and *RX*$^{Cre/+}$; *COUP-TFI*$^{F/F}$; *COUP-TFII*$^{F/F}$ double-gene mutant mice at 3W.
1180
1181 **Figure 3-source data 4.** The expression of HuB, Ctip2, and Prox1 in the hippocampus of the
1182 control and *RX*$^{Cre/+}$; *COUP-TFI*$^{F/F}$; *COUP-TFII*$^{F/F}$ double-gene mutant mice at 3W.
1183
1184 **Figure 3-figure supplement 1-source data 1.** The expression of GFAP, Nestin, and Dcx in
1185 the SGZ of vDG in the control and *RX*$^{Cre/+}$; *COUP-TFII*$^{F/F}$ mutant mice at 1M, in the SGZ of
1186 dDG in the control and *RX*$^{Cre/+}$; *COUP-TFI*$^{F/F}$ mutant mice at 1M, and in the SGZ of DG in
1187 the control and *RX*$^{Cre/+}$; *COUP-TFI*$^{F/F}$; *COUP-TFII*$^{F/F}$ double-gene mutant mice at 3W (part
1188 1).
1189
1190 **Figure 3-figure supplement 1-source data 2.** The expression of GFAP, Nestin, and Dcx in
1191 the SGZ of vDG in the control and *RX*$^{Cre/+}$; *COUP-TFII*$^{F/F}$ mutant mice at 1M, in the SGZ of

1192 dDG in the control and *RX*$^{Cre/+}$; *COUP-TFI*$^{F/F}$ mutant mice at 1M, and in the SGZ of DG in
1193 the control and *RX*$^{Cre/+}$; *COUP-TFI*$^{F/F}$; *COUP-TFII*$^{F/F}$ double-gene mutant mice at 3W (part
1194 2).
1195
1196 **Figure 3-figure supplement 1-source data 3.** The expression of GFAP and Nestin in the
1197 SGZ of vDG in the control and *RX*$^{Cre/+}$; *COUP-TFII*$^{F/F}$ mutant mice at 1M, in the SGZ of
1198 dDG in the control and *RX*$^{Cre/+}$; *COUP-TFI*$^{F/F}$ mutant mice at 1M, and in the SGZ of DG in
1199 the control and *RX*$^{Cre/+}$; *COUP-TFI*$^{F/F}$; *COUP-TFII*$^{F/F}$ double-gene mutant mice at 3W;
1200 quantitative analysis of GFAP/Nestin-positive cells in the SGZ of DG in the control and
1201 *RX*$^{Cre/+}$; *COUP-TFI*$^{F/F}$; *COUP-TFII*$^{F/F}$ double-gene mutant mice at 3W.
1202
1203 **Figure 3-figure supplement 1-source data 4.** The expression of GFAP, Nestin, and Dcx in
1204 the SGZ of vDG in the control and *RX*$^{Cre/+}$; *COUP-TFII*$^{F/F}$ mutant mice at 1M, in the SGZ of
1205 dDG in the control and *RX*$^{Cre/+}$; *COUP-TFI*$^{F/F}$ mutant mice at 1M, and in the SGZ of DG in
1206 the control and *RX*$^{Cre/+}$; *COUP-TFI*$^{F/F}$; *COUP-TFII*$^{F/F}$ double-gene mutant mice at 3W (part
1207 3); quantitative analysis of Dcx-positive cells in the SGZ of DG in the control and *RX*$^{Cre/+}$;
1208 *COUP-TFI*$^{F/F}$; *COUP-TFII*$^{F/F}$ double-gene mutant mice at 3W.
1209
1210 **Figure 4-source data 1.** The expression of Calretinin, Calbindin, and SMI312 in the ventral
1211 hippocampus of the control and *RX*$^{Cre/+}$; *COUP-TFII*$^{F/F}$ single-gene mutant mice at 1M.
1212
1213 **Figure 4-source data 2.** The expression SMI312 in the dorsal hippocampus of the control
1214 and *RX*$^{Cre/+}$; *COUP-TFI*$^{F/F}$ single-gene mutant mice at 1M, and the expression of Calretinin
1215 and Calbindin in the hippocampus of the control and *RX*$^{Cre/+}$; *COUP-TFI*$^{F/F}$; *COUP-TFII*$^{F/F}$
1216 double-gene mutant mice at 3W.

1217

1218 **Figure 4-source data 3.** The expression of Calretinin and Calbindin in the dorsal
1219 hippocampus of the control and *RX*$^{Cre/+}$; *COUP-TFI*$^{F/F}$ single-gene mutant mice at 1M, and
1220 the expression of SMI312 in the hippocampus of the control and *RX*$^{Cre/+}$; *COUP-TFI*$^{F/F}$;
1221 *COUP-TFII*$^{F/F}$ double-gene mutant mice at 3W.

1222

1223 **Figure 5-source data 1.** The expression of Lhx5 and Lhx2 in the telencephalon of the
1224 control and *RX*$^{Cre/+}$; *COUP-TFI*$^{F/F}$; *COUP-TFII*$^{F/F}$ double-mutant mice at E14.5; the
1225 expression of Tbr2 and NeuroD1 in the telencephalon of the control and *RX*$^{Cre/+}$; *COUP-*
1226 *TFI*$^{F/F}$; *COUP-TFII*$^{F/F}$ double-mutant mice at E14.5 (part 1).

1227

1228 **Figure 5-source data 2.** The expression of Sox2, Tbr2, and NeuroD1 in the telencephalon of
1229 the control and *RX*$^{Cre/+}$; *COUP-TFI*$^{F/F}$; *COUP-TFII*$^{F/F}$ double-mutant mice at E14.5.

1230

1231 **Figure 5-source data 3.** The expression profiles of genes involved in the hippocampal
1232 development of the control and double mutant mice at E11.5; the expression of Lhx5 and
1233 Lhx2 in the telencephalon of the control and *RX*$^{Cre/+}$; *COUP-TFI*$^{F/F}$; *COUP-TFII*$^{F/F}$ double-
1234 mutant mice at E11.5 and E13.5; the expression of Tbr2 and NeuroD1 in the telencephalon of
1235 the control and *RX*$^{Cre/+}$; *COUP-TFI*$^{F/F}$; *COUP-TFII*$^{F/F}$ double-mutant mice at E14.5 (part 2);
1236 quantitative analysis of Tbr2-positive and NeuroD1-positive cells in the hippocampal
1237 primordium of the control and *RX*$^{Cre/+}$; *COUP-TFI*$^{F/F}$; *COUP-TFII*$^{F/F}$ double-mutant mice at
1238 E14.5.

1239

1240 **Figure 5-figure supplement 1-source data 1.** Roles of *COUP-TFI* and *COUP-TFII* genes in
1241 the development and function of the hippocampus and the association with neurological
1242 disorders.

Figure 1, Yang et al.

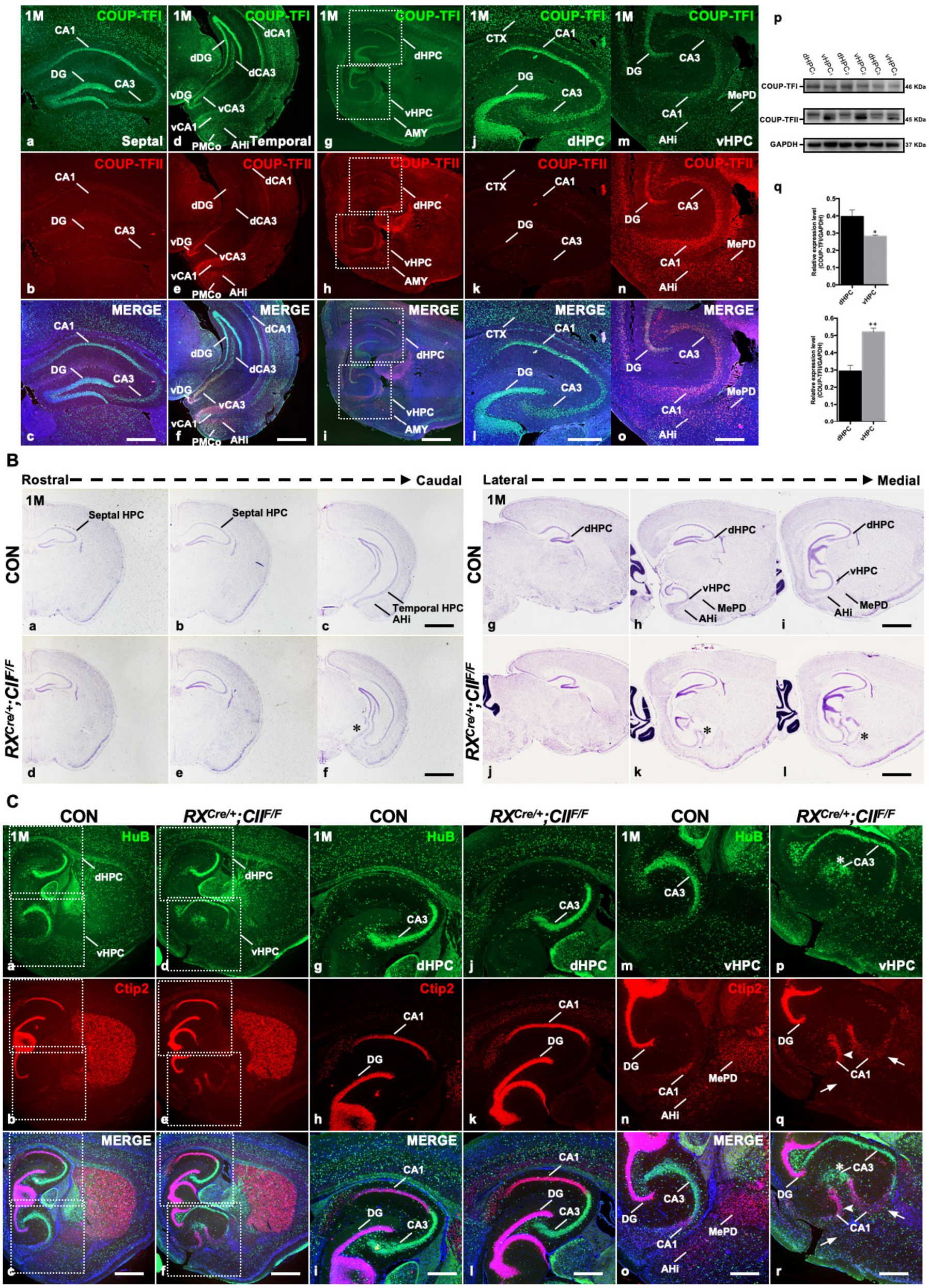

Figure 1—figure supplement 1, Yang et al.

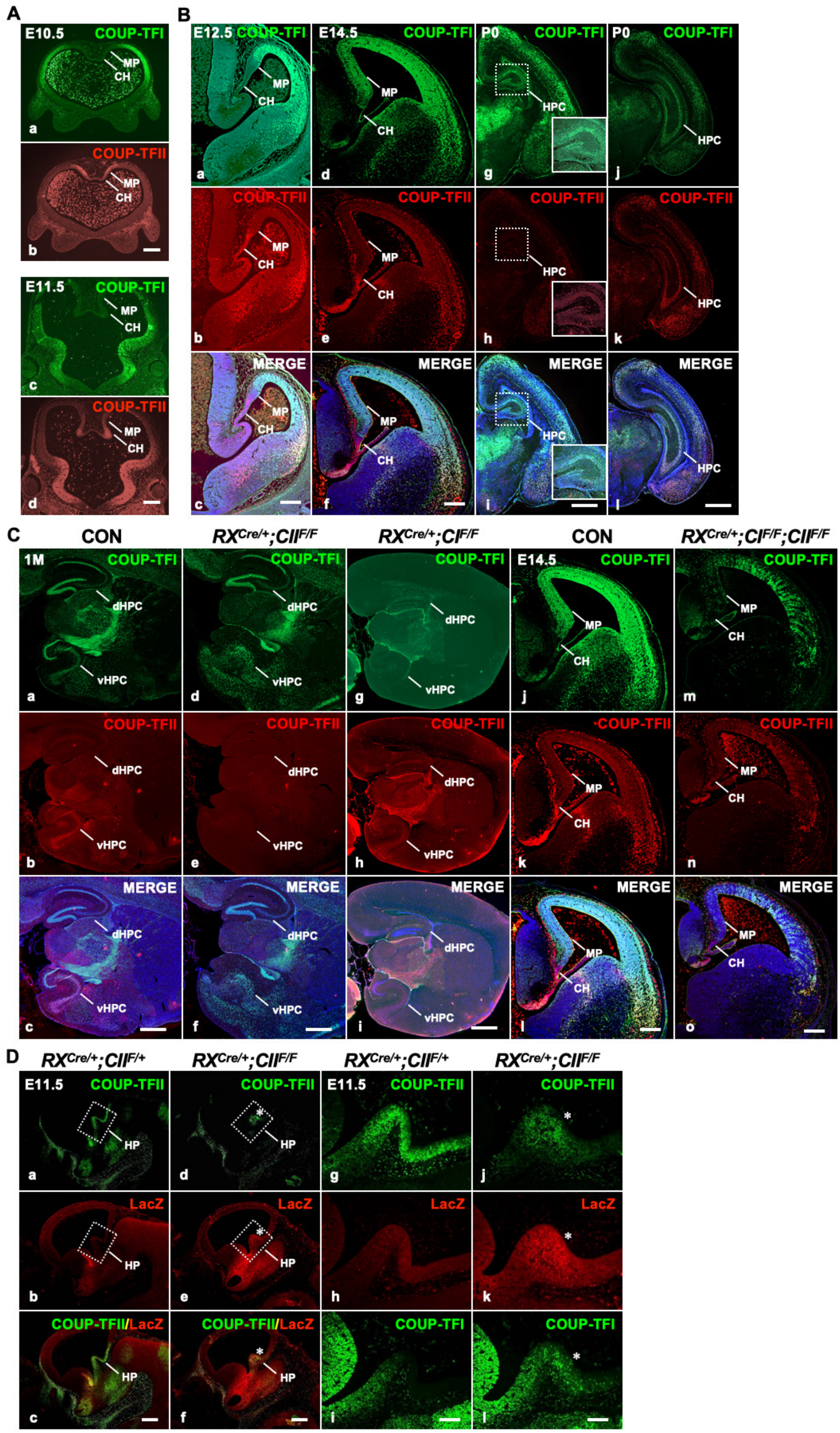

Figure 2, Yang et al.

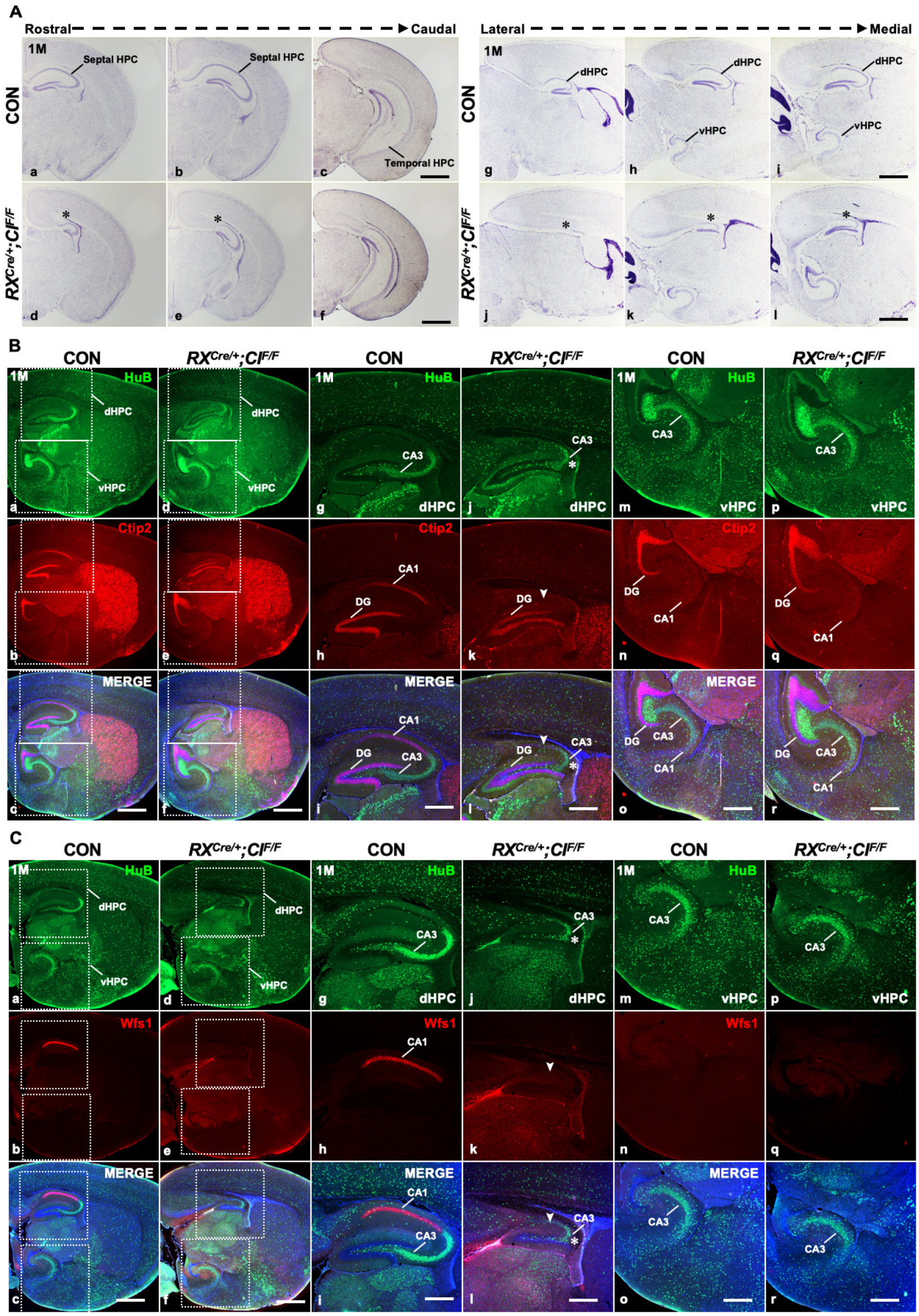

Figure 2—figure supplement 1, Yang et al.

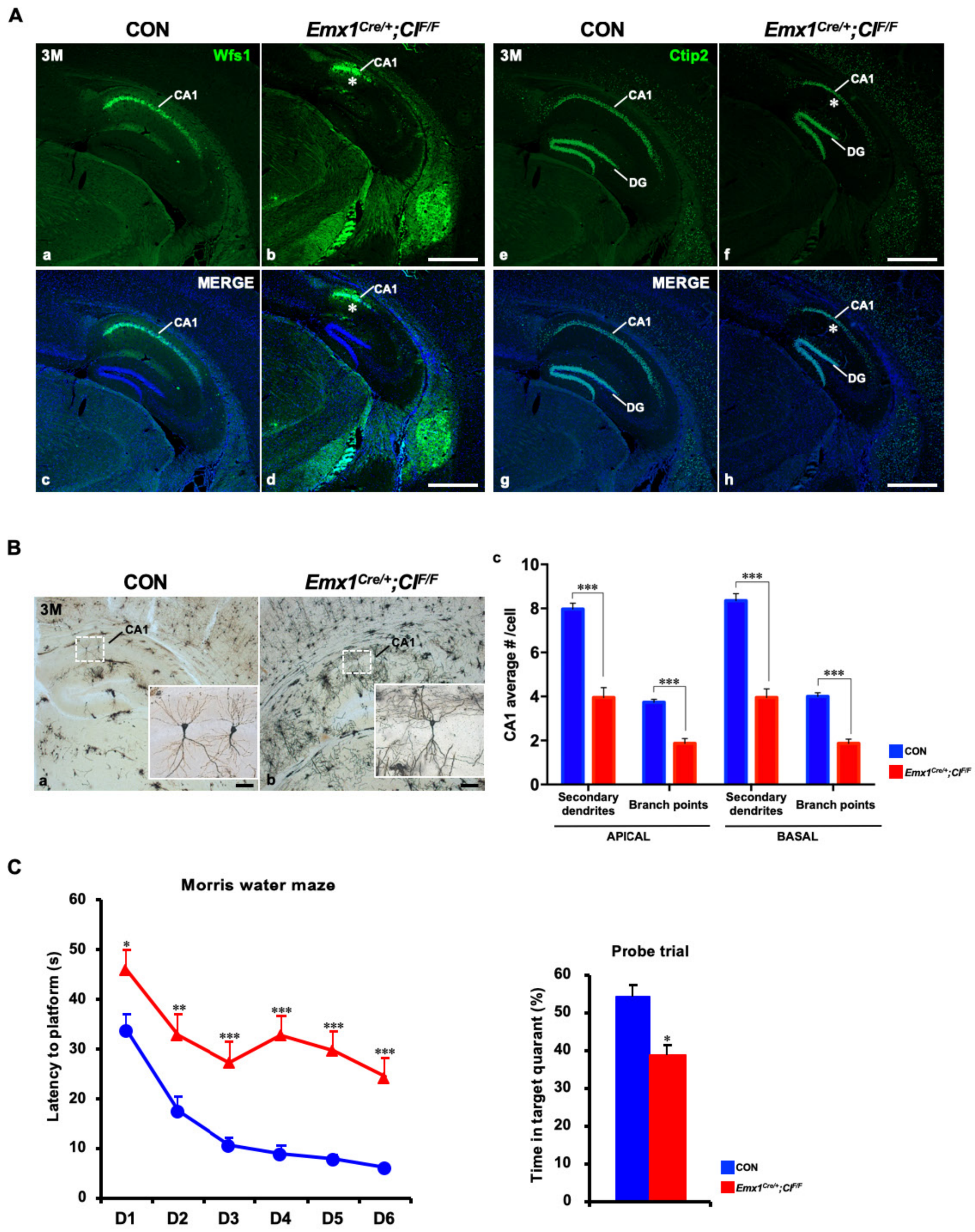

Figure 3, Yang et al.

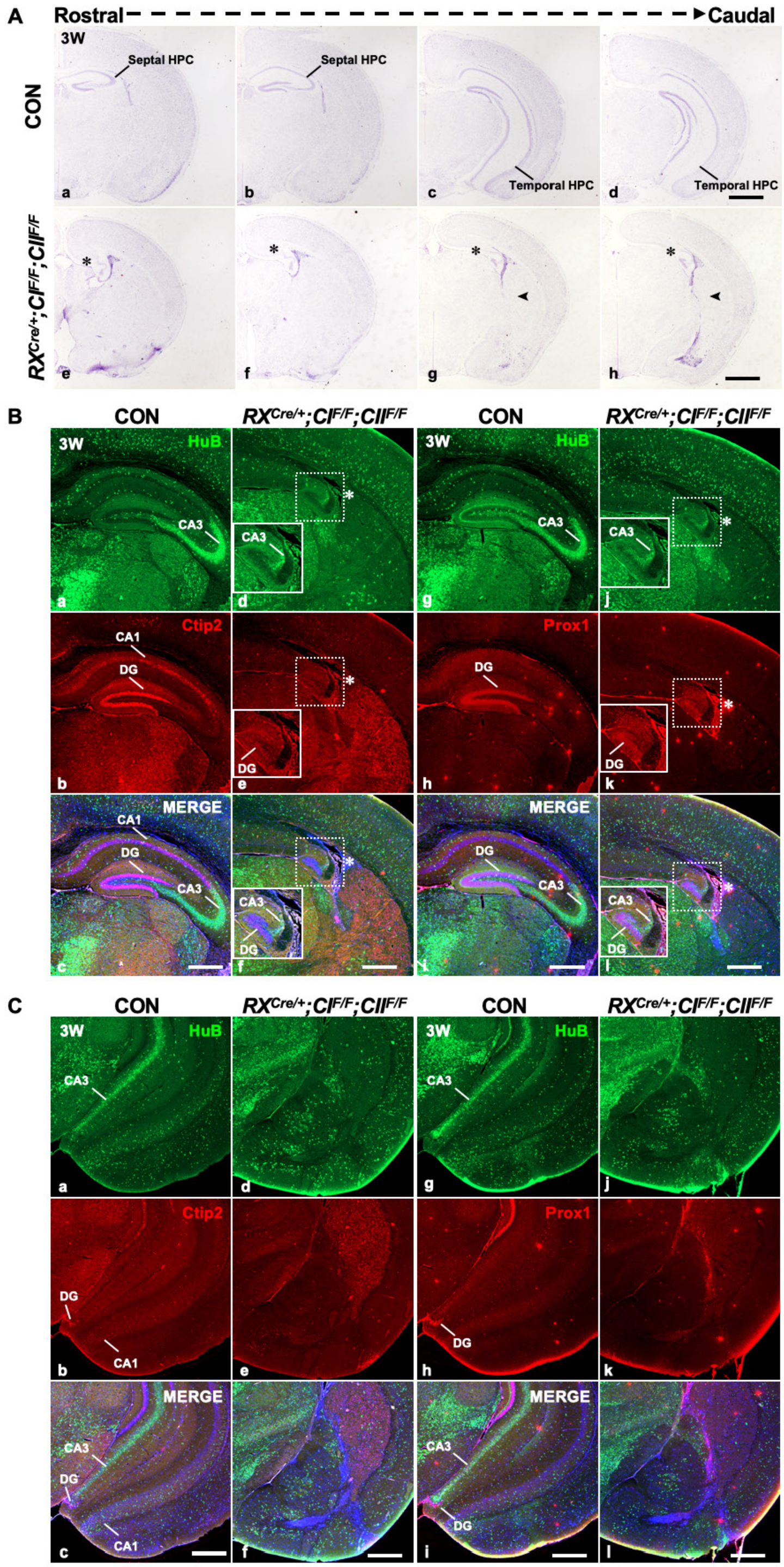

Figure 3—figure supplement 1, Yang et al.

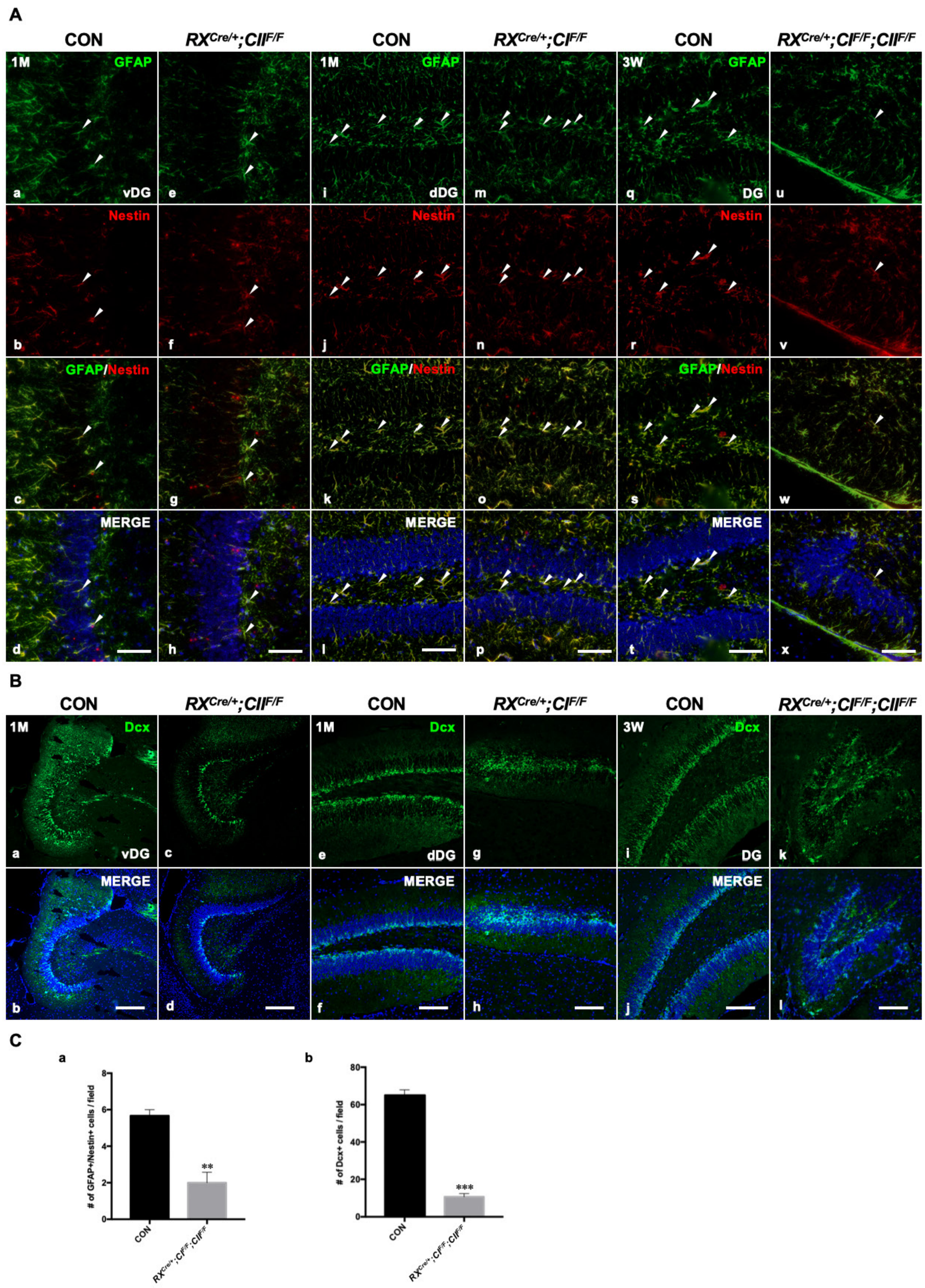

Figure 4, Yang et al.

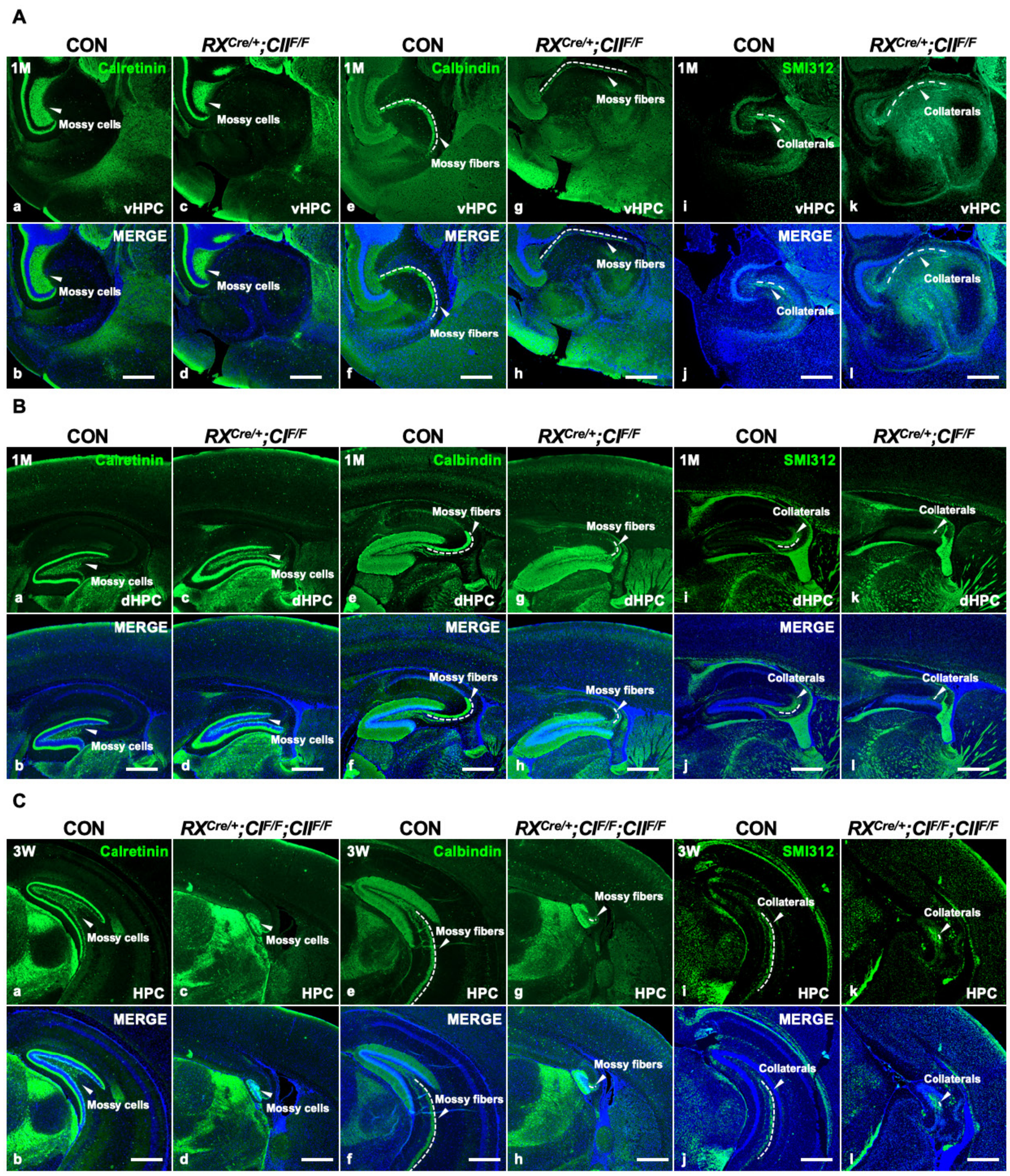

Figure 5, Yang et al.

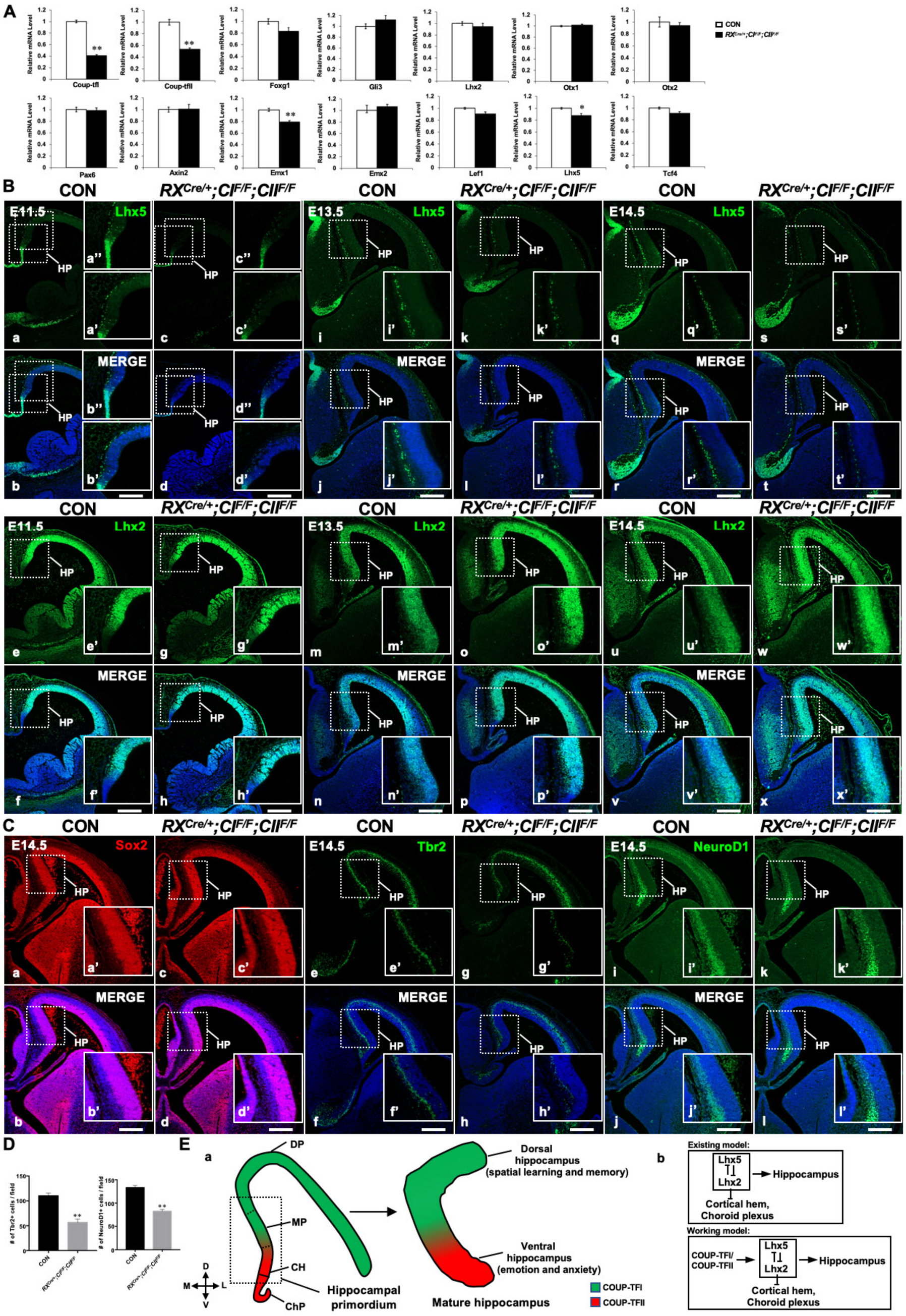
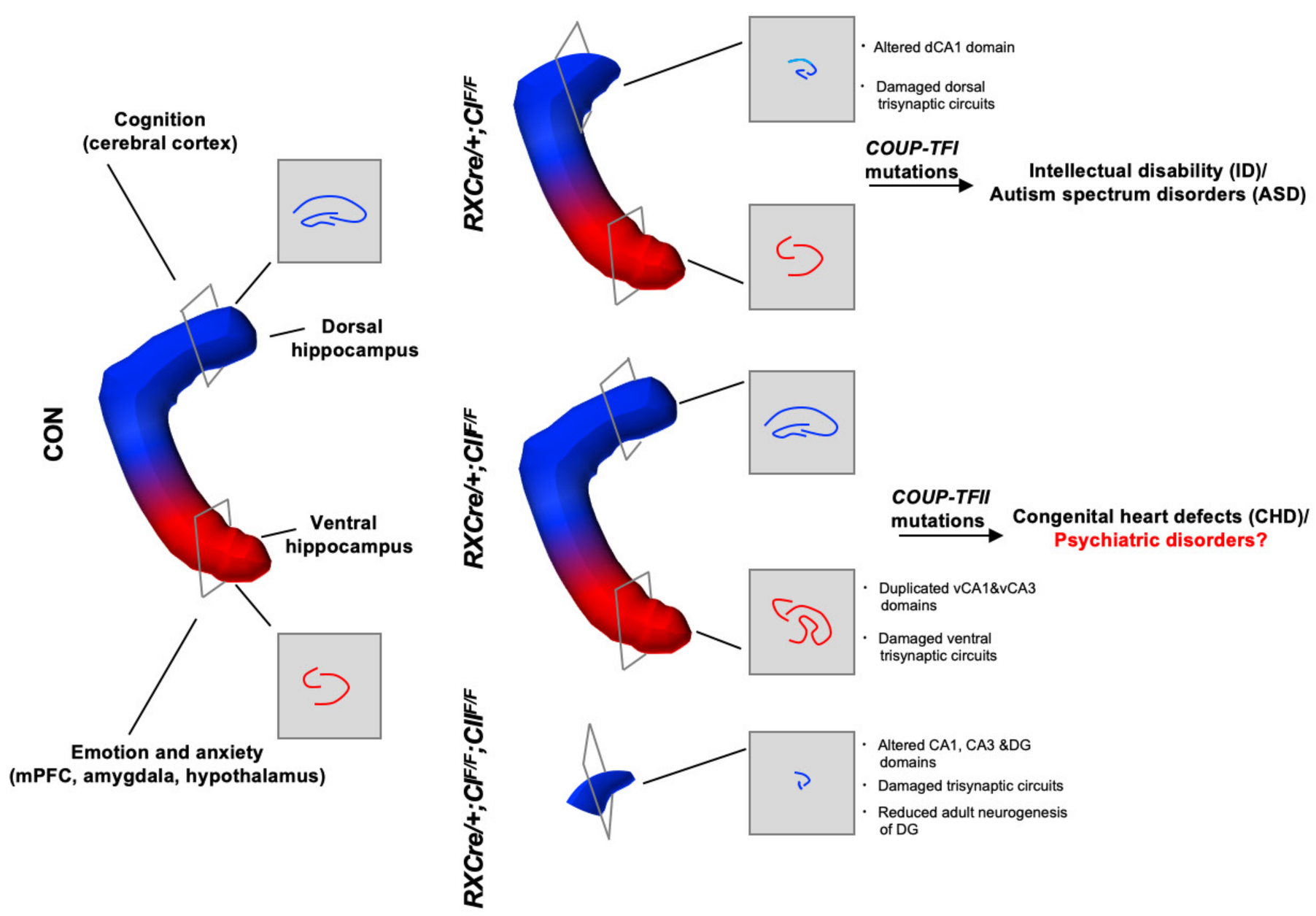
Figure 5—figure supplement 1, Yang et al.